Trehalose matrix effects on charge-recombination kinetics in Photosystem I of oxygenic photosynthesis at different dehydration levels

Marco Malferrari, Anton Savitsky, Mahir D. Mamedov, Georgy E. Milanovsky, Wolfgang Lubitz, Klaus Möbius, Alexey Yu. Semenov, Giovanni Venturoli

PII: S0005-2728(16)30521-7
DOI: doi: 10.1016/j.bbabio.2016.05.001
Reference: BBABIO 47686

To appear in: *BBA - Bioenergetics*

Received date: 18 December 2015
Revised date: 3 May 2016
Accepted date: 6 May 2016

Please cite this article as: Marco Malferrari, Anton Savitsky, Mahir D. Mamedov, Georgy E. Milanovsky, Wolfgang Lubitz, Klaus Möbius, Alexey Yu. Semenov, Giovanni Venturoli, Trehalose matrix effects on charge-recombination kinetics in Photosystem I of oxygenic photosynthesis at different dehydration levels, *BBA - Bioenergetics* (2016), doi: 10.1016/j.bbabio.2016.05.001

Trehalose matrix effects on charge-recombination kinetics in Photosystem I of oxygenic photosynthesis at different dehydration levels

Marco Malferrari[a], Anton Savitsky[b], Mahir D. Mamedov[c], Georgy E. Milanovsky[c], Wolfgang Lubitz[b], Klaus Möbius[b,d,*], Alexey Yu. Semenov[c,*], Giovanni Venturoli[a,e,*]

[a]Laboratorio di Biochimica e Biofisica Molecolare, Dipartimento di Farmacia e Biotecnologie, FaBiT, Università di Bologna, via Irnerio 42, I-40126 Bologna, Italy.

[b]Max-Planck-Institut für Chemische Energiekonversion, Stiftstr. 34-36, D-45470 Mülheim (Ruhr), Germany

[c]A.N. Belozersky Institute of Physical–Chemical Biology, Moscow State University, Moscow, Leninskie Gory, Moscow 119992, Russia

[d] Fachbereich Physik, Freie Universität Berlin, Arnimallee 14, D-14195 Berlin, Germany

[e]Consorzio Nazionale Interuniversitario per le Scienze Fisiche della Materia (CNISM), c/o Dipartimento di Fisica e Astronomia (DIFA), via Irnerio 46, Università di Bologna, I-40126 Bologna, Italy.

[*]Corresponding Authors:

K. Möbius, e-mail: moebius@physik.fu-berlin.de

A. Yu. Semenov, e-mail: semenov@genebee.msu.ru

G. Venturoli, e-mail: giovanni.venturoli@unibo.it

Abstract

Matrix effects on long-range electron transfer were studied in cyanobacterial Photosystem I (PS I) complexes, embedded into trehalose glasses at different hydration levels. W-band EPR studies demonstrated, via nitroxide spin probes, structural homogeneity of the dry PS I-trehalose matrix and no alteration of cofactors' distance and relative orientation under temperature and matrix variation. In dry trehalose glasses at room temperature (RT), PS I was stable for months. Flash-induced charge recombination kinetics were examined by high-field time-resolved EPR and optical spectroscopies. The kinetics in hydrated PS I-trehalose glasses mostly reflected the reduction of the photooxidized primary donor $P_{700}^{\bullet+}$ by the reduced terminal iron-sulfur clusters. Upon dehydration, the $P_{700}^{\bullet+}$ decay accelerated and became more distributed. Continuous distributions of lifetimes τ were extracted from the kinetics by two numerical approaches: a maximum entropy method (MemExp program) and a constrained regularization method (CONTIN program). Both analyses revealed that upon dehydration the contribution of the two slowest components (lifetimes τ ~300 ms and ~60 ms), attributed to $P_{700}^{\bullet+}$ $[F_A/F_B]^{\bullet-}$ recombination, decreased in parallel with the increase of the fastest component (τ ~150 µs), and of additional distributed phases with intermediate lifetimes. Dehydration at RT mimicked the effects of freezing water-glycerol PS I systems, suggesting an impairment of PS I protein dynamics in the dry trehalose glass. Similar effects were observed previously in bacterial reaction centers. The work presented for PS I provides new insights into the crucial issue of protein-matrix interactions for protein functionality as controlled by hydrogen-bond networks of the hydration shell.

Keywords: oxygenic photosynthesis, conformational dynamics, trehalose glassy matrices, charge recombination, cyanobacterial photosystem I.

Abbreviations: Chl, chlorophyll; DCPIP, 2,6-dichlorophenol-indophenol; DM, n-dodecyl-β-D-maltoside; PS I(tr) , trimeric Photosystem I; RC, bacterial reaction center; RT, room temperature.

Introduction

During the last decades, sugar-glass matrices attracted a growing interest in the biotechnology community for their ability to stabilize labile proteins, including therapeutic polypeptides, and optimize their storage at room temperature in the solid state [1-4]. Among other saccharides, trehalose (α-D-glucopyranosil α-D-glucopyranoside) forms, upon dehydration at room temperature (RT), glassy matrices which outstandingly protect the hosted protein against denaturation induced by freezing, heating, and drying (see trehalose structure in Fig. 1A). In nature, the bioprotective action of trehalose and other disaccharide glasses is used by several organisms able to survive for long periods (up to years) extreme draught and high temperatures by preserving the structural integrity of their cellular structures, while reversibly arresting their metabolism (anhydrobiosis) [5, 6].

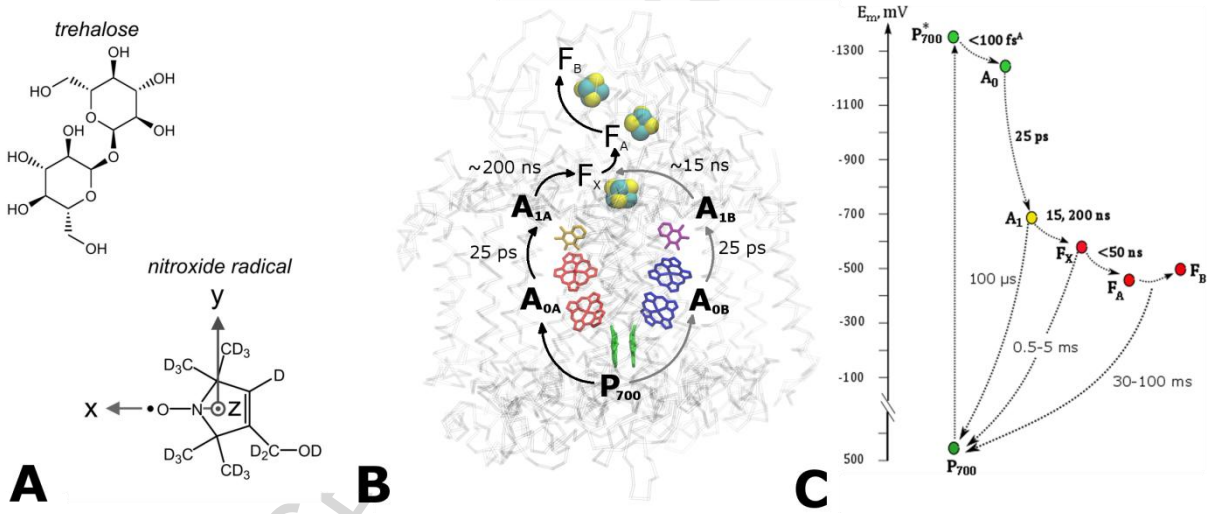

Figure 1. (A) Chemical structures of trehalose and the perdeuterated pyrroline type nitroxide radical. **(B)** Photosystem I structure and kinetics of forward electron-transfer reactions. Individual cofactors, P_{700}, A_{0A}, A_{0B}, A_{1A}, A_{1B}, F_X, F_A and F_B, are shown. **(C)** Energy diagram and lifetimes of forward and back electron-transfer reactions in PS I. See [25, 28, 30] for review. [A] The lifetime for the primary charge separation was detected under conditions of the RC chlorophylls' preferential excitation [7].

Although the molecular details of the protein-matrix dynamical coupling are still debated [8, 9], it is now well established that the extreme stabilization of proteins incorporated into trehalose glasses stems from the dramatic hindering of internal protein dynamics, which prevents loss of the native structure [10]. In particular, in dried trehalose-carboxy myoglobin glasses, Mössbauer and neutron scattering [11, 12], together with molecular dynamics simulations [13], demonstrated a strong reduction of the large-amplitude anharmonic motions associated with thermal interconversion among conformational substates. Additionally, the dynamics of the trehalose matrix and of the protein were found to be hindered in parallel when the content of residual water in the system was decreased.

When investigating the relationships between protein dynamics and function, the capability of dehydrated trehalose-water matrices of tuning the internal protein motions *at room temperature* offers distinctive advantages over low temperature studies in the hydrated system. In fact, freezing at cryogenic temperatures protein-water solutions in the presence of co-solvents, like glycerol, leads to the formation of glasses, mixing inevitably temperature and matrix effects. At variance, by controlling the hydration of trehalose matrices, protein dynamics can be retarded by orders of magnitude at constant (room) temperature, allowing to distinguish between temperature and matrix effects on protein reactivity driven by the internal protein motions. The potential of such an approach was first exploited by Eaton and co-workers [14, 15] who, by studying CO recombination after flash photolysis in carboxy myoglobin embedded in a RT trehalose glass, showed that protein-matrix interactions were primarily responsible for trapping of conformational substates and for inhibiting functionally important relaxations in the protein interior, independent of the temperature.

In previous years, we used extensively the incorporation of proteins into trehalose glasses to investigate the role of internal protein dynamics in long-range electron transfer within bacterial photosynthetic reaction centers (RCs). This integral pigment-protein complex represents the simplest photosystem which catalyzes the primary events of photosynthetic energy transduction. Hence, the RC is often used as a model complex suitable for elucidating light-induced electron-transfer processes in the more complex reaction centers of oxygenic photosynthesis. Within the RC from *Rhodobacter (Rb.) sphaeroides*, following light excitation, a bacteriochlorophyll *a* special pair (P) delivers an electron to the primary quinone acceptor Q_A, generating the charge-separated state $P_{865}^{\bullet+}Q_A^{\bullet-}$. The electron is subsequently transferred to a second ubiquinone-10 molecule, bound at the Q_B site, which acts as the terminal electron acceptor (for a review see [16]). From a driving-force assay it has been concluded that the latter reaction is conformationally gated, i.e., rate limited by a conformational change required before electron transfer [17]. In the absence of Q_B, the electron on $Q_A^{\bullet-}$ recombines by tunneling with the hole on $P_{865}^{\bullet+}$ [18].

In a previous study we found [19] that a progressive dehydration of the trehalose-RC glass, below ~0.07 g of water per g of dry matrix, first affects electron transfer from $Q_A^{\bullet-}$ to Q_B, causing its block in an increasing fraction of the RC population up to a complete RT arrest of the reaction over the whole RC population, similar to what is observed in water-glycerol mixtures at T < 200 K. We ascribed the reversible inhibition of electron transfer to Q_B in the trehalose glass to a large increase of the energy barriers between conformational substates which govern the transition probability for gated electron transfer [19]. Upon further dehydration (below ~0.03 g of water per g of dry matrix) the kinetics of $P_{865}^{\bullet+}Q_A^{\bullet-}$ recombination accelerate abruptly and become broadly distributed, mimicking, at RT, the kinetics observed at cryogenic temperatures (T < 100 K) in a glycerol-water mixture [19-21].

This similarity indicates that in RCs embedded in extremely dehydrated trehalose-water matrices thermal fluctuations between conformational substates, as well as relaxation from the *dark-adapted* to the *light-adapted* conformation [22, 23], are largely hindered at RT over the timescale (10^{-1} s) of charge recombination. We proposed that a network of hydrogen bonds, involving residual water molecules, connects the protein surface to the trehalose matrix, thereby determining a tight structural and dynamical coupling between the RC and the stiff water-sugar matrix [9, 10, 24].

In the present work, we have extended the study of trehalose-matrix effects to long-range electron transfer within Photosystem I (PS I), purified from the cyanobacterium *Synechocystis sp*. PCC 6803. This photosystem is characterized by a much higher structural and functional complexity as compared to the bacterial RC. By incorporating PS I into trehalose glasses at different hydration levels, we aimed at assessing and clarifying the role of the protein/solvent dynamics in governing specific intra-complex electron-transfer steps. Up to now this role has been hypothesized for certain PS I reactions on the basis of low temperature investigations, which suffer from the above mentioned difficulty of separating the temperature and matrix dependence of the electron transfer process. The room temperature "freezing" of conformational dynamics induced by dehydration within dried trehalose matrices represents an ideal tool to probe the static conformational heterogeneity which is expected to determine the electron transfer pathways and rates in such a complex photosystem.

PS I is a key pigment-protein complex of the electron-transfer chain of oxygenic photosynthetic organisms. It includes both a large antenna system for harvesting solar energy and a photochemical reaction center catalyzing stable charge separation across the membrane dielectric (for reviews, see [25-29]). The X-ray crystallographic structure of the cyanobacterial PS I (see Fig. 1B) has been resolved to 2.5 Å resolution [30], as a large trimeric complex (PS I(tr), ~1 MDa). The membrane embedded core of each PS I monomer is formed by the two largest subunits, PsaA and PsaB, which bind electron transfer cofactors arranged in two symmetrical branches A and B, extending from P_{700}, a pair of chlorophyll (Chl) *a* molecules located on the lumenal side, to the interpolypeptide [4Fe-4S] cluster F_X, placed on the opposite stromal side of the complex. Each of the two branches, related by a pseudo-C_2 rotation axis which passes through P_{700} and F_X, carries two monomeric chlorophyll *a* molecules (termed A_{0A} or A_{0B}) and one phylloquinone (A_{1A} or A_{1B}). At RT both branches are thought to be active in electron transfer [31] (for reviews see [32, 33] and references therein) with the ratio ~80:20% in favor of branch A in cyanobacterial PS I [34-36]. The degree of involvement of A and B branches into electron transfer in PS I from prokaryotic and eukaryotic photosynthesizing organisms still remains a matter of debate (reviewed in [33] and [32]). The terminal [4Fe-4S] clusters F_A and F_B are both bound to the peripheral protein subunit PsaC.

Following light excitation the excited singlet state of the primary electron donor, P_{700}^{*}, delivers an electron to the primary Chl acceptor A_{0A}/A_{0B} forming the charge separated state $P_{700}^{\bullet+}A_{0}^{\bullet-}$. The electron is then transferred in sequence to A_{1A}/A_{1B}, to the iron-sulfur cluster F_X, and ultimately to F_A/F_B. The rates of forward electron transfer are indicated in Figs. 1B and 1C (see [26, 29, 33] for review). When exogenous electron acceptors are not available, the electron on $(F_A/F_B)^{\bullet-}$ recombines with the hole on $P_{700}^{\bullet+}$ with lifetimes of 30-100 ms, while charge recombination from the $P_{700}^{\bullet+}F_X^{\bullet-}$ occurs with lifetimes of 0.5-5 ms. The back reaction from $P_{700}^{\bullet+}A_{1}^{\bullet-}$ takes place within ~100 µs (see Fig. 1C) [26, 33, 37]. Whereas the free energy difference ΔG of electron transfer between A_0 and A_1 was estimated to be >420 meV, the ΔG values of further electron transfer to the Fe_4S_4 clusters fall within 200 meV [32, 33, 38]. The forward reaction from A_1 exhibits a slow kinetic phase for electron transfer from A_{1A} to F_X, with a RT lifetime of ~300 ns and an activation energy of 110 meV, and a nearly temperature independent fast phase (τ~11-17 ns) of electron transfer from A_{1B} to F_X [34, 39] (see Fig.1B). The back reaction from $P_{700}^{\bullet+}A_{1}^{\bullet-}$ accelerates slightly (~1.5-fold) upon decreasing the temperature from 300 to 5 K [40]. At variance, F_X recombination is most probably thermally activated, as it is suggested to occur via the intermediate $P_{700}^{\bullet+}A_{1}^{\bullet-}$ state [25, 26, 41]. Recombination from the F_A/F_B clusters was found to be temperature-dependent with an activation energy of ~200 mV [42].

Time-resolved EPR and optical studies revealed a complex behavior of low-temperature PS –I photochemistry, characterized by heterogeneity with respect to electron transfer. In particular, illumination at 77 K led to virtually irreversible charge separation between P_{700} and F_A/F_B, in a fraction of the PS I population [43]. In the remaining photoactive subpopulation, the dominating charge recombination occurred from the $P_{700}^{\bullet+}A_{1}^{\bullet-}$ state [40, 44], with a minor contribution from the $P_{700}^{\bullet+}F_X^{\bullet-}$ state [44, 45], suggesting a heterogeneous inhibition of forward electron transfer to the iron-sulfur acceptors. To explain the low-temperature observations, mechanisms were proposed in which the conformational dynamics of a statically heterogeneous PS I complex conditions electron transfer to the iron-sulfur acceptors [25].

We have tested and investigated at RT the coupling between electron transfer and protein-solvent dynamics by incorporating PS I into trehalose glasses at different hydration levels. Preliminary attempts to study the effect of trehalose glass on the kinetics of charge recombination in PS I were reported previously in the form of abstracts [46, 47]. In the first part of the present work, by using high-field EPR and FTIR spectroscopy we show that functional PS I complexes can be embedded into a structurally and dynamically homogeneous trehalose matrix, which does not significantly distort the molecular configuration of the $P_{700}^{\bullet+}A_{1}^{\bullet-}$ radical pair. Subsequently, the kinetics of charge recombination after a pulsed excitation, consistently probed by time resolved EPR and optical NIR absorption

spectroscopy, have been examined as a function of the hydration of the matrix. The study of charge recombination reactions has provided new information also on the mechanism of forward electron transfer steps to the iron-sulfur acceptors, showing that these processes are critically coupled to the protein/solvent conformational dynamics, being suppressed when the latter are strongly reduced at room temperature by dehydration of the trehalose matrix: Dehydration of the trehalose-PS I glass blocks electron transfer to F_A/F_B, and, under the most dehydrated conditions, also to the F_X acceptor. When comparing the matrix-effects observed in trehalose-PS I and trehalose-RC glasses, it appears that the control of forward electron transfer to the terminal electron acceptors (iron-sulfur centers or the quinone Q_B, respectively) by conformational reorganization is a common property of both photosystems. Taken all results together, we can say that the work presented provides new insights into the important issue of protein-matrix interactions for protein functionality as controlled by hydrogen-bond networks. In trehalose, they lead to a high rigidity of the protein-matrix complex, coming along with extreme stability already at room temperature. Naturally, further studies are needed on this issue, e.g., regarding the molecular interactions to be in control of how deep the rigidity of the trehalose matrix propagates to immobilize the binding sites of the various electron-transfer cofactors inside the protein complex. Work in this direction is in progress in our laboratories.

2 Materials and Methods

2.1 Cell growth and isolation of PS I complexes

A glucose-tolerant strain of *Synechocystis sp.* PCC 6803 was grown at 30°C in BG-11 medium under light. Cyanobacterial cultures in late exponential phase were pelleted by centrifugation, washed twice with BG-11 medium, and suspended in 50 mM TRIS buffer (pH 8.1). PS I trimeric complexes were isolated using n-dodecyl-β-D-maltoside (DM) and sucrose gradients as described earlier [48]. The isolated PS I preparation was resuspended in 50 mM Tris buffer (pH 8.1), containing 0.03% (w/v) DM, frozen as small aliquots with a chlorophyll *a* concentration of 2 mg mL^{-1} in liquid nitrogen, and stored at -90°C. Chlorophyll was extracted from PS I trimers with 80% acetone and determined as described in [49].

2.2 Sample preparation and determination of residual water in trehalose-PS I matrices

Trehalose (>99% purity) was used as supplied by Sigma-Aldrich. The perdeuterated form of the nitroxide radical (3-hydroxymethyl-2,2,5,5-tetramethylpyrrolin-1-oxyl) was synthesized as described previously [50] and kindly provided by Herbert Zimmermann (Max-Planck Institute for Medical Research, Heidelberg, Germany). Its molecular structure is shown in Fig. 1A.

Trehalose-PS I glassy matrices were prepared following essentially the procedures for the incorporation of bacterial RCs into trehalose glasses [51], except for lowering the protein concentration in the starting liquid mixture to optimize simultaneously W-band EPR and optical

measurements in samples of comparable composition. For measuring the kinetics of $P_{700}^{\bullet+}$ decay after a laser pulse, trehalose-PS I glasses were prepared from a 30-40 μL drop of an aqueous solution of 50 mM TRIS-HCl, pH 7.5, 0.03% (w/v) DM, 782 mM trehalose, and PS I corresponding to a final Chl-a concentration of 1.1 mM. This yielded a (trehalose/PS I(tr)) molar ratio of $2.0 \cdot 10^5$. Transient W-band EPR signals of the spin-correlated $P_{700}^{\bullet+}A_1^{\bullet-}$ radical pair were acquired in trehalose-PS I matrices characterized by a (trehalose/ PS I(tr)) molar ratio of $1.0 \cdot 10^5$ obtained from a drop containing 545 mM trehalose and 1.5 mM PS I Chl-a. To maintain the primary electron donor pre-reduced during the vitrification process, 5 mM Na-ascorbate and 5 μM 2,6-dichlorophenol-indophenol (DCPIP) were added to all these liquid samples.

Trehalose-PS I glasses containing the pyrroline type nitroxide radical were obtained from aqueous drops with a volume of 20-30 μL. In order to examine matrices with a (trehalose/ PS I(tr)) molar ratio varied over a large range (from $6.0 \cdot 10^4$ to $5.4 \cdot 10^5$) but keeping the (trehalose/nitroxide radical) molar ratio constant, different compositions of the starting solution were chosen. The final concentration of trehalose, PS I Chl-a, and nitroxide radical were varied in the following ranges: 370-384 mM, 0.35-1.93 mM, and 0.92-1.61 mM, respectively. This resulted in a (trehalose/nitroxide) molar ratio of ~400.

Vitrification was carried out by drying at RT the trehalose-PS I liquid drop, deposited on a 50 mm diameter CaF_2 window, under N_2 flow inside a desiccator for about 4 hours, as described in [52]. Controlled dehydration/rehydration of the obtained glassy matrices was achieved by the isopiestic method [53]. The optical window on which the solid amorphous sample was formed, was exposed to the desired value of relative humidity *r* by placing it inside a gastight sample holder, containing at the bottom about 1.5 mL of the appropriate saturated salt solution. The following saturated solutions were employed to obtain at 297 K the *r* values indicated in brackets [54]: NH_4NO_3 (63%), $Mg(NO_3)_2$ (53%), K_2CO_3 (43%), $MgCl_2$ (33%), LiCl (11%). Both the determination of the residual water contents (see below) and the time-resolved optical absorption measurements (see section 2.4) were performed directly on the sample which was exposed to the saturated atmosphere inside the holder. For EPR measurements, on the other hand, the dehydrated, fragile trehalose-PS I glasses, prepared as described above, were crumbled into small fragments, which could be inserted into the cylindrical quartz capillaries (0.6 mm I.D.) for the W-band EPR cavity. To expose the EPR sample to the required relative humidity, a drop of the appropriate saturated salt solution was inserted into the capillary. It was then sealed and equilibrated for three days before the measurements, as described in [51].

The water content of the matrices was evaluated from the area under the ($\nu_2+\nu_3$) NIR combination band of water at 5155 cm^{-1}, using an absorptivity value [55] of 102 absorbance unit nm M^{-1} cm^{-1}, and following essentially the procedure previously used for trehalose-RC glassy matrices

[20] and RC films [53]. In contrast to the latter system in the case of trehalose-PS I glasses the direct use of a chlorophyll band (e.g., the band at 784 nm) as an internal standard was prevented by the excessive absorbance of the sample, due to the much larger number of chlorophyll molecules per complex. As an internal standard we chose, therefore, the area of the NIR trehalose band at 4760 cm^{-1} that is attributed to combinations of OH stretching and C-O-H bending modes [56, 57]. The absorptivity of this band was determined by examining a series of trehalose-RC glasses of known trehalose/RC molar ratios. As internal reference the absorption of the RC bacteriochlorophyll band at 802 nm was chosen for which an extinction coefficient of 288 ± 14 mM^{-1} cm^{-1} was used [58]. Our measurements on six glasses, differing also in the hydration level, yielded for the trehalose band an absorptivity value (average ± standard deviation) of $(3.3 \pm 0.3)\cdot 10^2$ nm M^{-1} cm^{-1}.

The FT-NIR absorption measurements for determining the water content of the matrices were performed with a Jasco Fourier-transform 6100 spectrometer, equipped with a DLATGS detector, as described in [53]. The hydration of the matrix is given primarily as (H_2O/trehalose) molar ratio. We report the hydration state also as (mass of H_2O/ mass of dry matrix). Since the fraction of residual water, which partitions between the protein-matrix interface and the bulk trehalose matrix, is not known, the water content expressed as (mass of H_2O/ mass of dry matrix) allows a physically meaningful comparison of the overall matrix hydration between various trehalose-protein glasses which differ in the sugar/protein ratio and/or in the nature of the embedded protein (e.g., RC [20, 21, 24, 52], carboxy myoglobin [12], lysozyme [59]). The dry matrix includes trehalose, the protein complex, and the detergent belt in the case of integral membrane protein complexes. For trehalose-PS I glasses, we have assumed a molecular mass of the PS I trimer of 1.05 MDa and a detergent belt around PS I(tr) formed by 10^3 n-dodecyl β-D-maltoside molecules [60].

2.3 W-band EPR measurements

High-field EPR measurements were performed with a laboratory-built spectrometer operating at a microwave (mw) frequency of 95 GHz (W-band) and an external magnetic field B_0 of 3.4 T. The spectrometer is optimized for cw and pulse experiments, as described previously [61-63]. In cw EPR experiments B_0 was modulated at 8 kHz with an amplitude of 30 μT. Low mw power (< 1μW) incident on the critically coupled cavity (mw field amplitude $\omega_1 < 1.5\cdot 10^5$ $rad\cdot s^{-1}$) was chosen to avoid saturation. For optical sample irradiation the light was guided to the center of the cavity through a quartz fiber of 0.8 mm diameter. The electron transfer was initiated by singlet excitation of the primary donor P_{700} at 532 nm using a frequency-doubled Nd:YAG laser (5 ns pulse length, 1-10 Hz repetition rate, 0.5 mJ/pulse on the sample surface). The transient EPR signals of the short-lived spin-correlated radical pair $P_{700}^{\bullet+}A_1^{\bullet-}$ were acquired employing the mw pulse sequence for primary electron spin-echo (ESE) generation. It was applied 400 ns after pulsed laser excitation of P_{700}: $(t_p)_{x,-x}$-τ-$(2t_p)$-τ-echo. The

pulse length t_p of the $\pi/2$ mw pulses was generally set to 30 ns. To acquire field-swept ESE detected spectra the pulse separation time τ was fixed to 150 ns. The charge-recombination kinetics data were obtained for $P_{700}^{\bullet+}$ with thermally equilibrated spin polarization by recording its transient EPR absorption, after a laser flash, using 30 kHz field modulation and lock-in detection with different time resolutions (from 50 µs to 10 ms). The EPR kinetics were acquired using different repetition frequencies of the exciting flash (always lower than 1 Hz), and up to single shot without averaging for time scales above 1 s. Temperature control was achieved by a gas-flow cryostat housing the cavity probehead. Simulation procedures and analysis of the nitroxide radical EPR spectra were performed using the EasySpin toolbox for the Matlab program package [64].

2.4 Time-resolved near-infrared optical spectroscopy

The kinetics of charge recombination were studied by recording the transient absorption changes of P_{700} at 820 nm. They were measured from the µs to second time range using a single-beam spectrometer of local design. The measuring beam (25 mW output power), provided by a L808P200 diode laser (Thorlabs, Newton, NJ, USA), after crossing the sample, was focused on a reverse-biased PIN silicon photo diode, matched to a transimpedance amplifier (Thorlabs, PDA36A) with 17 MHz bandwidth. The detector was protected from scattered excitation light by a long-pass glass filter (Oriel 51350), with a cut-on wavelength of 780 nm. Although the time rise of the detector was estimated ~20 ns, this was not reached because of a stray-light artefact of the excitation laser pulse. This allowed us to monitor reliably the decay of absorption transients due to P_{700} photoxidation only for $t \geq 30$ µs.

Transients of the output voltage signal were digitized and averaged by a LeCroy 9410 digital oscilloscope controlled by an Olivetti M290 personal computer. Each decay kinetics was obtained by acquiring two kinetic traces consisting of 10^4 values sampled every 1 µs and 0.1 ms, respectively. The non-overlapping parts of these traces were combined to yield the overall decay. Typically 64 and 36 signals were averaged on the fast and slow sweep, respectively. During averaging, a dark time of 1 minute was allowed between successive flash excitations, in order to assure a complete relaxation of the system.

The excitation beam was provided by a sulforhodamine B dye cavity (Pulsed Dye Laser RDP-1, Radiant Dyes Laser GmbH, Wermelskirchen, Germany), emitting at 587 nm. It was pumped by a frequency-doubled Q-switched Nd:YAG laser (Handy 710, Quanta System, Milano, Italy) delivering 45 mJ pulses of 7 ns width at 532 nm. The resulting photoexcitation energy at 587 nm, measured on the sample surface, was 8 mJ. The CaF_2 window on which the trehalose-PS I glasses were formed was oriented at 45° with respect to both the measuring and excitation beam to minimize laser light reflection towards the detector. Measurements on PS I solutions were performed in a quartz cuvette with 2 mm optical path length. In order to reduce the O_2 concentration in the sample, a small volume

(53 μL) of a concentrated suspension containing 1.2 mM of PS I Chl-a, 330 mM TRIS-HCl, pH 7.5, 0.52% (w/v) n-dodecyl β-D-maltoside, 66 mM Na-ascorbate, 66 μM DCPIP was added to 647 μL of water extensively bubbled with Argon gas and the cuvette was tightly sealed with a Teflon cap.

2.5 Numerical analysis of recombination kinetics

In the analysis of complex decay kinetics, regularization algorithms that yield quasi-continuous lifetime distributions offer a significant advantage over the commonly used unconstrained best fitting, based on non-linear least-squares (χ^2) minimization, of the experimental data to the sum of discrete exponential processes, because the number of kinetic phases does not need to be specified in advance. Two approaches were employed in the present study, the Tikhonov-Phillips regularization [65], implemented in the program CONTIN [66], and the Maximum Entropy method, used in the program MemExp (version 4.0) [67, 68].

In essence, CONTIN minimizes the sum of the squares of the second differences (discretized form of the second derivative) of the distribution, while MemExp maximizes the Shannon informational entropy of the distribution, while minimizing the reduced χ^2 of the corresponding kinetics. For both algorithms the solution obtained with a given quality of fit (sum of residuals) is unique.

The regularizator used by CONTIN "binds" together adjacent exponential components, smoothing the resulting sum spectrum, which is a reasonable assumption in biological systems, where distributed kinetics are expected. CONTIN initially creates the reference solution with ordinary least-squares algorithms, which typically leads to overfitting of the data noise. Then for each of the produced solutions with different regularization values CONTIN calculates the probability that the tested solution is worse than the reference one (in terms of χ^2 between the solution and the data) due to random noise alone. The solution with this probability closest to 0.5 is then selected in accordance with the original approach [66].

MemExp determines the lifetime distribution by an iterative, second-order optimization of the entropy S, subject to constrained values of the χ^2. The constrained optimization is essentially achieved by maximizing the function $Q=S-\lambda\chi^2$, where λ is a Lagrange multiplier. During Newton-Raphson optimization of Q followed by adjustment of the Lagrange multiplier, the lifetime distribution evolves from a flat distribution into a series of maximum-entropy distributions which become progressively structured as χ^2 decreases. In the iterative calculation the selected distributed fit is the last for which both χ^2 and the correlation length of the residuals have decreased by more than 1% from the preceding distribution [67]. A detailed MemExp documentation can be found at https://cmm.cit.nih.gov/memexp/memexp_4pt0/.

Both methods, when discretizing the integral of the continuous lifetime distribution (see eq. 1 in section 3.3) calculate the experimental kinetics as a sum of a large number of exponential decays (80 in case of CONTIN and 180 in case of MemExp), characterized by lifetimes linearly distributed in the logarithmic scale. The lifetime distributions obtained were decomposed into a sum of Gaussian phases using locally developed non-linear minimization routines based on modified Marquardt and grid search algorithms [69]. The contributions of the individual phases are given as the fractional area under the corresponding Gaussian sub-distributions.

3 Results and Discussion

3.1 Dehydration/rehydration of trehalose-PS I matrices under controlled relative humidity

Previous studies have demonstrated that the structural and dynamical organization of trehalose amorphous matrices depends critically upon their hydration state [51], and that this parameter in turn strongly affects the dynamical coupling between the embedded protein and the matrix (for a review, see [9]). The determination of the residual water content in the protein-disaccharide glass, and a reliable control of its hydration state, play therefore a pivotal role for any matrix-effect study. As described in section Material and Methods, we have determined the content of residual water by FT-NIR spectroscopy. We controlled the hydration state of the trehalose-PS I glasses over a wide range by exposing the system to an atmosphere of definite relative humidity *r*, obtained by gaseous equilibration with different saturated salt solutions.

Figure 2 shows the time course of the water content of a trehalose-PS I matrix during incubation at $r = 11\%$, followed by its rehydration upon successive exposures at increasing relative humidity, from $r = 33\%$ to $r = 63\%$. The kinetics of dehydration is strongly non-exponential: Dehydration to $\sim 9 \cdot 10^{-2}$ g of H_2O per g of dry matrix (corresponding to ~1.8 water molecules per trehalose) occurs in about two days. Subsequent incubation at $r = 11\%$ causes a very slow further release of water leading, after about three months, to a steady level of $\sim 2.5 \cdot 10^{-2}$ g of H_2O per g of dry matrix (corresponding to ~0.5 water molecules per trehalose). Nonexponential kinetics, previously reported for polymeric and amorphous systems, have been proposed to reflect diffusion limited desorption processes (see [48] and reference therein). Besides this nonexponential character, the extremely slow dehydration phase observed in the trehalose-PS I glass appears to reflect the release of a water population strongly bound to the bulk sugar matrix and/or to the protein-detergent complex.

When switching from $r = 11\%$ to $r = 33\%$, the hydration of the sample increases monotonically reaching a steady value in about 6 days. At variance, following the transitions to higher relative humidity values, the time course of the hydration levels exhibits spikes, which increase in amplitude upon increasing the *r* values. It appears that under these conditions transient hydration levels,

exceeding the ones reached at equilibrium, are attained, possibly due to the different time-scales over which water adsorption at the surface and diffusion inside the bulk glass occurs.

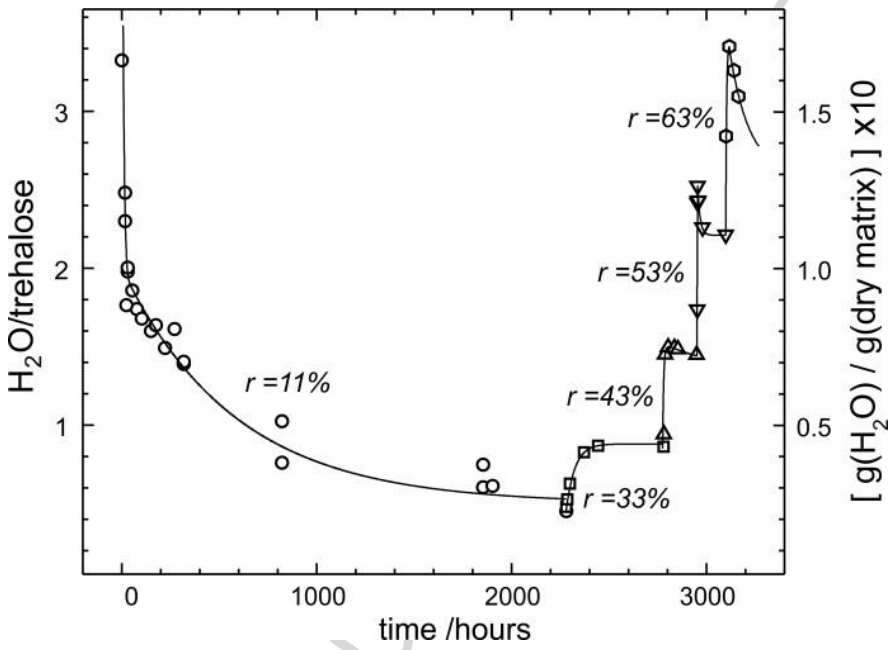

Figure 2. Dehydration/rehydration kinetics of trehalose-PS I glassy matrices, characterized by a molar ratio of $2.0 \cdot 10^5$ for (trehalose/PS I(tr)). After dehydration to a relative humidity $r = 11$ % (circles), the sample was rehydrated by incubation at increasing r values ($r = 33\%$, squares; $r = 43\%$, triangles; $r = 53\%$, inverted triangles; $r = 63\%$, diamonds). The content of residual water is expressed as (H_2O/trehalose) molar ratio on the left scale, and as mass of water per mass of dry matrix (trehalose plus PS I detergent complex) on the right scale.

A water absorption isotherm can be obtained from the equilibrium hydration values of Fig. 2 (see Fig. S3 in Supplementary material). Upon decreasing the relative humidity from $r = 63\%$ to $r = 33\%$, the residual water content of the matrix decreases almost linearly by ~0.11 g of H_2O per g of dry matrix, while further dehydration to $r = 11\%$ leads to a much smaller decrease, i.e., by ~0.02 g of H_2O per g of dry matrix. The change in slope of the equilibrium absorption isotherm occurs at water contents which correspond to the slow phase of the dehydration kinetics (see Fig. 2), supporting the view that below $r = 33\%$ (i.e., below ~0.05 g of H_2O per g of dry matrix) a hindered release of tightly bound water molecules takes place.

The equilibrium hydration level at $r = 11\%$ (~0.5 H_2O/trehalose) compares well with those determined at the same r value in binary trehalose-water glassy matrices [51] and in a trehalose-RC glass with a sugar/protein molar ratio of $5 \cdot 10^3$ [52]. This suggests that, at high sugar/protein molar

ratios and low values of relative humidity, the presence of a large protein complex like the PS I trimer has only negligible effect on the affinity of the matrix for water.

3.2 Structural and dynamical characterization of trehalose-PS I glassy matrices by EPR

As discussed in the Introduction section, high-field W-band EPR spectroscopy is distinguished over standard X-band EPR by providing valuable high-resolution information on the structural and dynamical organization of binary disaccharide-water systems even in the amorphous solid state [51]. Analysis of the room-temperature EPR spectrum of a nitroxide radical dissolved in a dehydrated trehalose matrix, equilibrated at r = 11%, has demonstrated that upon extensive dehydration trehalose forms a highly homogeneous amorphous phase in which the residual water and hosted nitroxide molecules are uniformly distributed. Additionally, it has been shown that the rotational mobility of the guest nitroxide probe is dramatically restricted at RT, to an extent comparable to that observed at cryogenic temperatures (T <150 K) [51]. The incorporation of a protein within the trehalose glass can in principle perturb the structural and dynamical characteristics of the matrix, e.g., by affecting its homogeneity, particularly in the case of a large integral membrane protein, such as the trimeric PS I surrounded by its detergent belt. Therefore, we have compared the W-band EPR spectra of perdeuterated nitroxide radicals dispersed in dehydrated trehalose matrices in the absence and in the presence of embedded PS I(tr) complexes, varying the sugar/protein molar ratio.

Figure 3A compares the W-band high-field EPR spectra of perdeuterated nitroxide radicals measured at RT in a pure trehalose glass and in a trehalose-PS I matrix, characterized by a (trehalose/PS I(tr)) molar ratio $m = 1.8 \cdot 10^5$, both samples dehydrated at a relative humidity r = 11%. At the high Zeeman field of W-band EPR, the three B_0 regions, corresponding to the principal values of the g-tensor (i.e., g_{xx}, g_{yy}, g_{zz}), are well resolved, and the nitrogen ^{14}N hyperfine splitting into three lines is observed both in the g_{yy} and g_{zz} spectral regions. The essentially coinciding lineshapes of the spectra measured in the absence and in the presence of PS I clearly indicate that the nitroxide radicals are exposed to identical microenvironments and that the nitroxide probe molecules are comparably immobilized.

The microenvironment of the nitroxide spin-probe is highly homogeneous, as follows from the fact that each EPR spectrum can be simulated using a unique set of magnetic interaction parameters (g_{ii}, A_{ii}). The spectra were calculated by solving numerically the spin Hamiltonian including nuclear Zeeman and quadrupole terms. A multi-parameter fitting of the calculated spectra to the observed ones yields, as unique solution, the g and A tensors' principal values g = [2.0082; 2.0060; 2.0024] and A = [0.58; 0.58; 3.75] mT. They coincide within error margins with the values obtained from the spectra recorded in the absence or presence of PS I, see Fig. 3. From this we infer that the incorporation of PS

I does not perturb the homogeneous structural organization of the trehalose matrix in terms of distribution of the hosted spin-probe and residual water molecules.

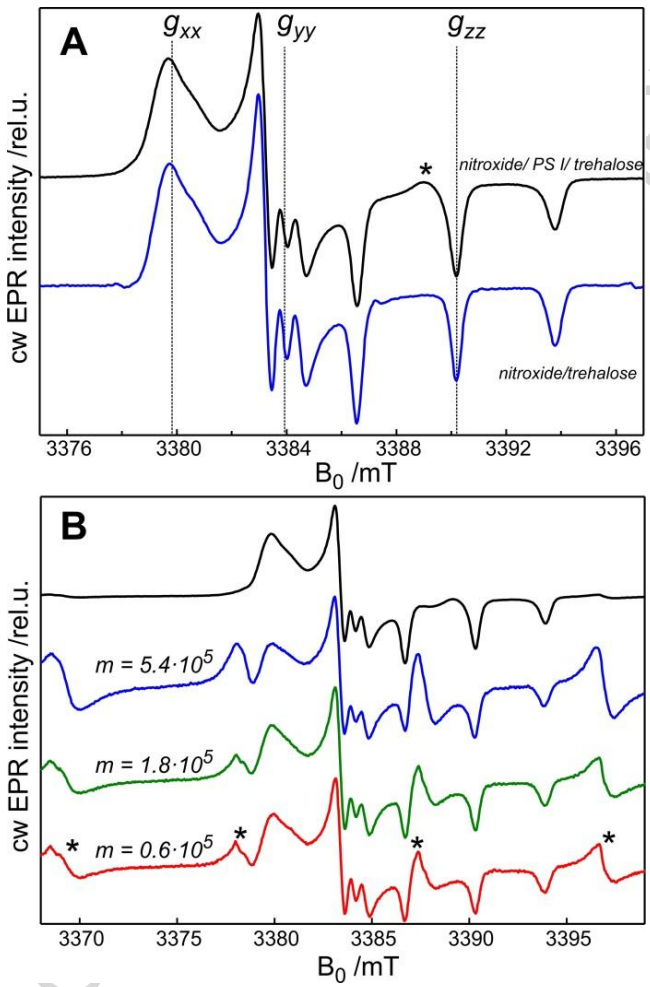

Figure 3. (A) W-band cw EPR spectra of the perdeuterated nitroxide radical dispersed in trehalose matrices in the presence (upper trace) and absence (lower trace) of embedded PS I complexes, recorded at 293 K. The trehalose-PS I glass has a molar ratio of $1.8 \cdot 10^5$. Both samples have been dried by incubation at r = 11%. The trehalose-PS I glassy matrix was prepared without sodium ascorbate and DCPIP. The asterisk marks the position of the EPR signal of residual $P_{700}^{\bullet+}$. **(B)** W-band cw EPR spectra of the nitroxide radical diluted in a series of trehalose-PS I matrices, equilibrated at r = 11%, characterized by different (trehalose/PS I(tr)) molar ratios, as indicated in the figure. The spectra have been measured in trehalose-PS I matrices prepared in the presence of 5 mM Na-ascorbate and 5 μM DCPIP, except for the spectrum shown at the top of the panel. The asterisks mark the EPR line positions of Mn^{2+} in the PS I complex. All measurements were performed at 293 K.

These conclusions have been confirmed by studying a series of trehalose-PS I glasses characterized by sugar/protein molar ratios m ranging between $0.6 \cdot 10^5$ and $5.4 \cdot 10^5$ (see Fig. 3B). Besides changing the values of m, we also amended the PS I suspension, from which glasses were

formed, by sodium ascorbate and DCPIP (see Materials and Methods). These reducing agents have been used at the appropriate concentrations when studying the kinetics of charge-recombination processes after a laser pulse in trehalose-PS I matrices (see also section 3.3). This was done in order to fully reduce the primary electron donor cation $P_{700}^{\bullet+}$ in the dark, thus obtaining fully photoactive samples. By applying the same reducing procedure for measuring the EPR spectra of the nitroxide radical we aimed at probing the structural and dynamic characteristics of the trehalose-PS I matrices under the same conditions prevalent in the optical kinetic experiments.

The addition of the reducing agents had, however, a drawback: it caused a strong decrease of the amplitude of the nitroxide EPR signal, due to partial reduction of the nitroxide radical to diamagnetic hydroxylamine. In spite of this, as shown in Fig. 3B, informative spectra of the spin probe could be observed with a rather good signal-to-noise ratio. The fraction of nitroxide radicals, which survived the sample preparation procedure in the presence of sodium ascorbate and DCPIP, can be estimated to ~5%. This was evaluated by comparing the nitroxide EPR signal intensity with the EPR signals of Mn^{2+} stemming from a manganese contamination of the PS I preparation. The prominent contribution of Mn^{2+} EPR signals is observable in all the spectra of Fig. 3B. The lineshape of the nitroxide EPR signals does not change significantly at the different trehalose/PS I(tr) molar ratios. This shows that in the tested range the molar ratio has no effect on the microenvironment of hosted spin probe and its rotational dynamics. In summary: Figures 2 and 3 show that the inclusion of the large trimeric PS I complex in the solid trehalose matrix does not perturb significantly the hydration state as well as the structural and dynamical organization of the homogeneous trehalose glass at $r = 11\%$ over a wide range of PS I concentrations.

A second point we have addressed concerns the reverse side of the mutual protein-matrix interaction discussed so far, i.e., the possibility that the extensively dehydrated, stiff trehalose matrix perturbs in turn the structure of the PS I complex, altering in particular distance and relative orientation of its cofactors. Obviously, such structural matrix effects would be relevant for the kinetics of electron-transfer processes. The structural configuration of two key cofactors of the PS I complex, i.e., the primary donor P_{700} and the quinone acceptor A_1, can be conveniently probed by examining the spin-polarized EPR spectrum of the radical pair created in the pure singlet electronic state taken before thermalization of the spin system has occurred, i.e., before Boltzmann equilibrium of the spin populations has been reached. Electron spin polarization can be observed by transient EPR methods provided the lifetime of the radical pair and/or the electron spin-lattice relaxation times of the individual pair partners are long enough compared to the EPR detection time [70]. This polarization phenomenon is well accounted for by the correlated-coupled-radical-pairs (CCRP) model [70, 71]. In solid amorphous samples, the transient EPR lineshape, determined by the magnitude and sign of the

dipolar coupling of the two electron spins, is sensitive to the relative orientation and distance of the radical-pair partners. A lineshape analysis reveals, therefore, these important structural parameters of the donor-acceptor spin system.

In Fig. 4 the W-band EPR spectra of the spin-correlated radical pair $P_{700}^{\bullet+}A_1^{\bullet-}$, as measured in a dehydrated trehalose-PS I matrix at 293 K and 120 K, are compared with the spectrum recorded in an aqueous buffer solution of PS I frozen at 120 K. The three spectra are essentially identical, revealing that the structural configuration of the transient radical pair does not change significantly upon solvation in the different matrices embedding the PS I complex. This conclusion is in line with the results of our previous study of bacterial RCs which had shown the absence of matrix effects on the EPR spectrum of the spin-correlated $P_{865}^{\bullet+}Q_A^{\bullet-}$ radical pair generated by pulsed light excitation of RCs embedded in trehalose glasses [72]. Taken together, these observations suggest that in photosystems of different size and complexity regarding subunit composition and oligomeric organization, the molecular configuration of the cofactors involved in the primary processes of charge separation is not significantly distorted by incorporation into trehalose glass, even under extensive dehydration.

In view of studying the effect of the matrix hydration level on the charge-recombination kinetics (see Fig. 6 below and section 3.3) we examined a possible dependence of the $P_{700}^{\bullet+}$ decay kinetics on the trehalose/PS I(tr) molar ratio *m*, covering the same range used in the analysis of nitroxide spin-probe spectra. Figure 5A compares the $P_{700}^{\bullet+}$ decays after laser-pulse photoexcitation, plotted on a linear timescale, as measured by transient W-band EPR, in trehalose-PS I matrices with different molar ratio values *m*. The measurements were performed on the same glassy matrices used for recording the spectra of the nitroxide spin-probe shown in Fig. 3B. Variation of the sugar/protein molar ratio between $m = 0.6 \cdot 10^5$ and $m = 5.4 \cdot 10^5$ has essentially no effect on the kinetics. This is confirmed by Fig. 5B in which the decay trace, plotted on a logarithmic timescale, of $P_{700}^{\bullet+}$ in a trehalose-PS I matrix for $m = 1.8 \cdot 10^5$ is compared with that for $m = 1.0 \cdot 10^5$. The latter glassy sample was formed in the absence of the nitroxide radical. The identity of the two kinetic traces additionally shows that the EPR spin-probe does not perturb the kinetics of $P_{700}^{\bullet+}A_1^{\bullet-}$ charge recombination.

The results presented so far show that dry trehalose-PS I glasses, equilibrated at $r = 11\%$ and characterized by *m* values in the 10^4-10^5 range, represent a homogeneous amorphous system which is well defined in terms of hydration. Remarkably, the embedded PS I complexes fully retain their photoactivity at RT and preserve it for long periods of time (at least for two months).

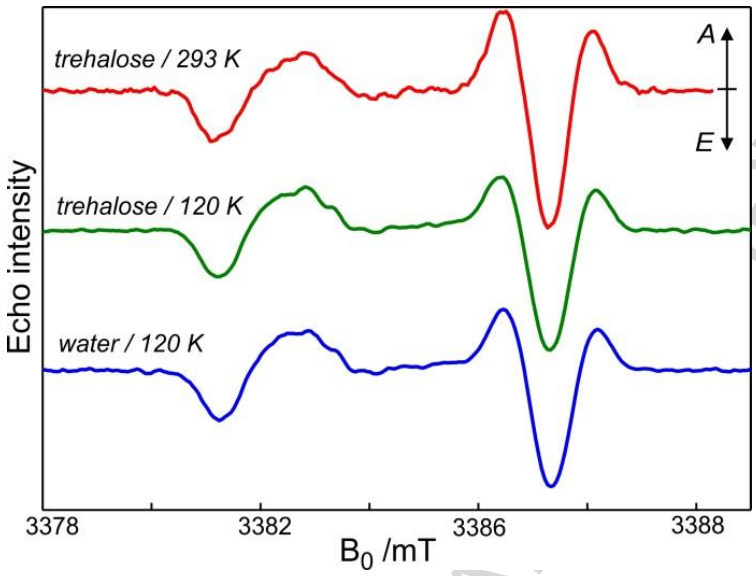

Figure 4. Field-swept echo-detected W-band EPR signals of the spin-correlated $P_{700}^{\bullet+}A_1^{\bullet-}$ radical pair in dark-adapted PS I complexes, embedded in trehalose glassy matrices and dissolved in water. The spectra were recorded 400 ns after a 532 nm laser flash using a Hahn echo pulse sequence with π/2 pulse length of 30 ns and interpulse delay of 150 ns. The signals were acquired at both 293 K (upper spectrum) and 120 K (middle spectrum), as well as in water at 120 K (lower spectrum). The trehalose-protein matrix was characterized by a (trehalose/PS I(tr)) molar ratio of $m = 1.0 \cdot 10^5$. The $A_1^{\bullet-}$ contribution to the spectrum is at the low-field side (higher *g* values than the $P_{700}^{\bullet+}$ contribution). ***A*** stands for absorptive and ***E*** for emissive type of spin polarization.

The kinetics of $P_{700}^{\bullet+}$ decay after pulsed photoexcitation are also independent of the protein concentration in the glassy matrix over the *m* range examined. The described trehalose-protein system appears, therefore, to be well-suited for investigating the effects of matrix hydration on the kinetics of charge-recombination processes. The hydration state of the matrix is known to govern the dynamical properties of the glassy system [51, 73-75]. Such hydration effects largely modulate the protein-matrix coupling, as was shown earlier for a simpler photosynthetic protein system like the bacterial RC [19-21, 24, 76].

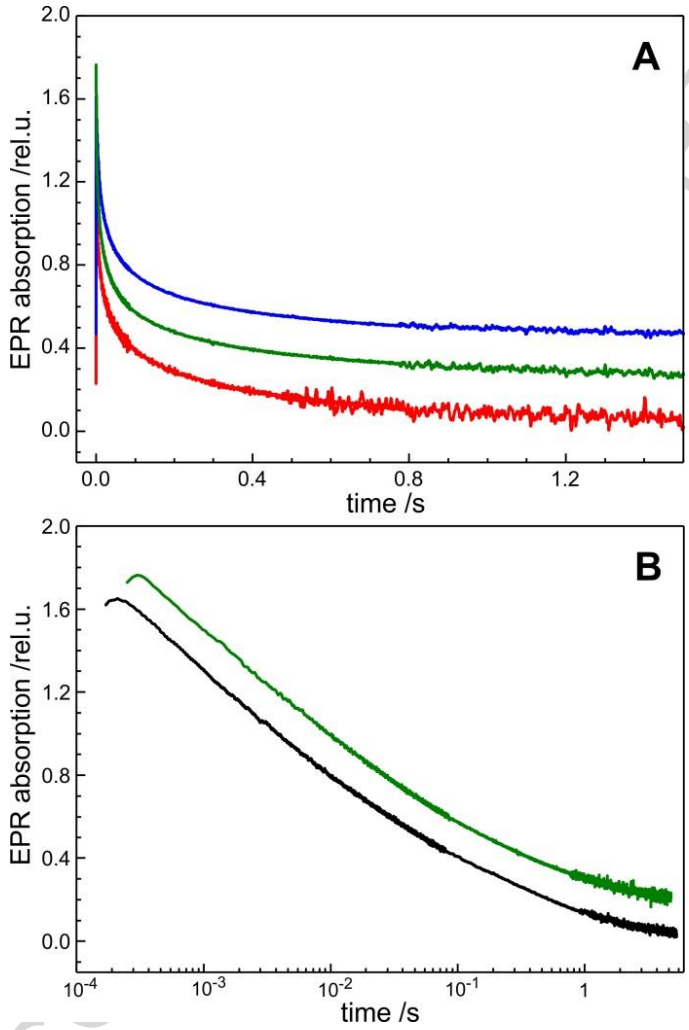

Figure 5. Kinetics of $P_{700}^{\bullet+}$ decay in PS I complexes embedded into trehalose matrices equilibrated at r = 11%, measured at RT by transient W-band EPR following a single 532 nm laser pulse. The kinetic decay traces were acquired at the maximum EPR absorption of the thermally equilibrated $P_{700}^{\bullet+}$ cofactor. Traces have been offset for better visual clarity. **(A)** Kinetics recorded in trehalose-PS I matrices at $m = 0.6 \cdot 10^5$ (blue trace), $m = 1.8 \cdot 10^5$ (green), and $m = 5.4 \cdot 10^5$ (red). Glasses were formed in the presence of the pyrroline type nitroxide radical at a (trehalose/nitroxide) molar ratio of ~400. **(B)** Kinetics measured in trehalose-PS I glasses at $m = 1.8 \cdot 10^5$ (green trace) and $m = 1.0 \cdot 10^5$ (black). For the latter matrix the nitroxide radical was omitted. Lock-in detected transient EPR signals were obtained using a different time resolution for the different time windows (i.e., 50 μs for 0 < t < 100 ms; 1 ms for 100 ms < t < 900 ms; 10 ms for 900 ms < t < 5s). Note the logarithmic time scale.

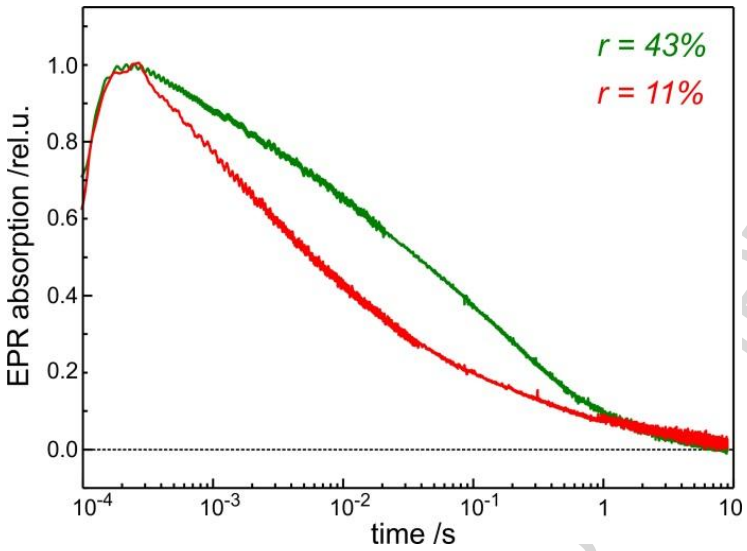

Figure 6. The effect of the hydration level of the trehalose/PS I glass on the kinetics of $P_{700}^{\bullet+}$ decay measured at RT by transient W-band EPR following a single 532 nm laser pulse. The matrix was characterized by $m = 2.0 \cdot 10^5$ and prepared in the absence of the nitroxide radical. Signals were acquired using different time resolutions in the different time windows, as detailed in the legend of Fig. 5B. Trehalose-PS I glasses have been incubated at r = 11% (red trace) and r = 43% (green trace).

The kinetics of charge recombination within PS I complexes embedded in trehalose matrices are indeed strongly affected by the hydration level of the system. Figure 6 compares the kinetics of $P_{700}^{\bullet+}$ decay following a laser pulse in trehalose-PS I matrices equilibrated at different relative humidity values, r = 11% and r = 43%. The traces have been normalized to their maximal amplitude which is reached about 200 μs after the photoexcitation pulse due to the time response of the lock-in detected EPR signals. Although kinetic information before this time lag is experimentally not accessible by our EPR set-up, it is clear that dehydration of the glass from r = 43% to r = 11% leads to an overall strong acceleration of the charge-recombination processes after the light flash. It also appears that, similar to what is observed in PS I solutions [37], the recombination kinetics extend at least over more than three orders of magnitude, and include phases distributed on different timescales.

The large dehydration-induced acceleration of the transient-EPR detected charge-recombination kinetics prompted us to systematically study its dependence on the hydration level of the PS I-trehalose glass with better time resolution. To this end, we have chosen to record the decay of $P_{700}^{\bullet+}$ after a laser pulse by optical absorption spectroscopy, rather than by transient EPR, in view of (a) the better time resolution of about 20 μs; (b) the possibility of evaluating, in parallel with kinetic measurements, the residual water content of the matrices, equilibrated at different relative humidity values, by NIR spectroscopy using the water ($\nu_2+\nu_3$) combination band. The water content could not so easily be estimated directly by this approach in the 0.6 mm cylindrical sample capillaries used for

the W-band EPR measurements, because of problems with light scattering by the sample fragments present in the narrow capillaries (see Materials and Methods).

3.3 The effect of dehydration on the charge-recombination kinetics in trehalose-PS I glasses

Figure 7 shows the decay of $P_{700}^{\bullet+}$ after a laser pulse, as measured at RT by the optical absorption change at 820 nm, in solution and in a trehalose-PS I glassy matrix at different hydration levels. The matrix has been dehydrated by equilibration at r = 11% (see Fig. 2) and progressively rehydrated up to r = 63%. To test data reproducibility, additional trehalose-PS I glasses have been prepared and equilibrated at selected r values between 11% and 63%. The obtained kinetics of $P_{700}^{\bullet+}$ decay were very similar to those of Fig. 7 at the corresponding relative humidity. Reproducible kinetics were also obtained by transient EPR, as shown by $P_{700}^{\bullet+}$ decays measured in several glassy samples. An example is provided by the signals of Fig. 5, which have been acquired at r = 11% in different matrices, which differ also in the sugar/protein molar ratio.

As expected from the EPR results (see Fig. 6), the hydration of the matrix dramatically affects charge recombination. While incorporation into a wet matrix (r = 63%) has a small effect, dehydration from r = 63% to r = 11% decreases the overall half-time of the decay by two orders of magnitude. Because of the lower time resolution of transient EPR, a precise comparison between the kinetics acquired by EPR (see Fig. 6) and by NIR absorption spectrometry (see Fig. 7) is problematic. Particularly for the fastest decay (r = 11%), an accurate determination of the maximal EPR signal amplitude at t = 0 is not feasible. Nevertheless, the overall acceleration of recombination kinetics, when dehydrating from r = 43% to r = 11%, is similar in both experiments (as judged from the half-time of the decays), demonstrating that the dehydration effect is consistently probed by EPR and optical spectroscopy. Our attempt to overlay corresponding decay traces acquired by the two methods through appropriate normalization (not shown) confirms this agreement. It indicates, however, slightly slower EPR decays under the driest conditions (r = 11%). We suppose that this is due to a slightly higher value of r reached during incubation with saturating salt solutions in the narrow EPR capillaries than that obtained within the wider sample holder for optical measurements.

For analyzing the $P_{700}^{\bullet+}$ decay kinetics we have been guided by the following considerations:

(a) Previous studies of PS I solutions at RT showed that a description of the recombination kinetics in terms of discrete exponential decays requires several kinetic phases that have been attributed to the recombination of $P_{700}^{\bullet+}$ with the acceptor anions from $P_{700}^{\bullet+}A_1^{\bullet-}$, $P_{700}^{\bullet+}F_X^{\bullet-}$ and $P_{700}^{\bullet+}[F_A/F_B]^{\bullet-}$ [37]. Each of these back-reactions exhibits a biexponential character, suggesting the presence of different PS I conformational states [37]. The large conformational heterogeneity of PS I, giving rise to multiphasic kinetics, has been additionally revealed by low-temperature investigations (see e.g., [40, 44]).

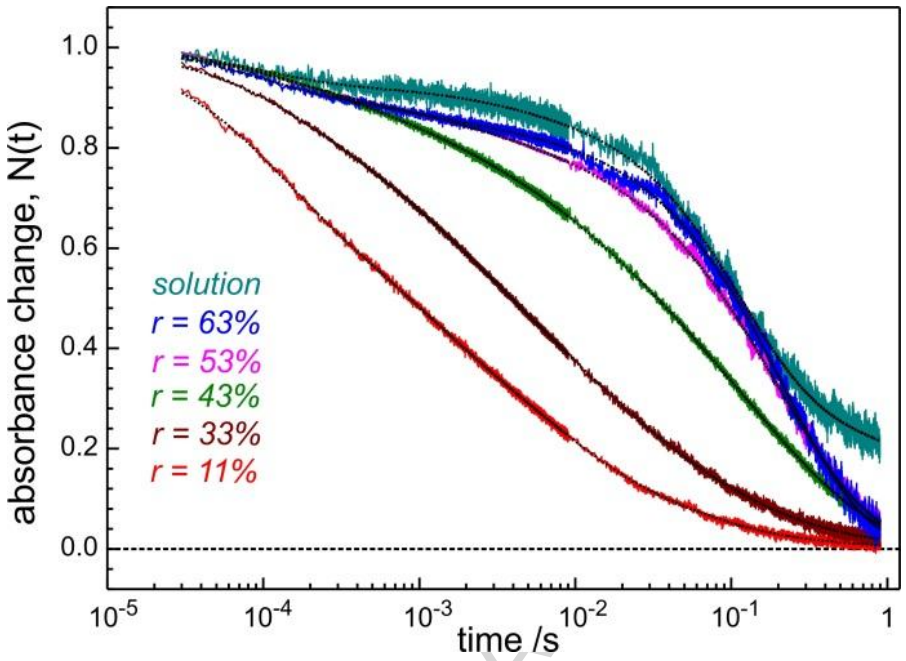

Figure 7. Decay kinetics *N(t)* of $P_{700}^{\bullet+}$ following PS I photoexcitation by a laser pulse, as measured by NIR absorption spectroscopy in solution and in a trehalose-PS I glassy matrix equilibrated at different values of relative humidity *r*. The matrix was characterized by a trehalose/PS I(tr) molar ratio $m = 2.0 \cdot 10^5$. Transient absorption changes, measured at 820 nm, have been normalized to the maximum amplitude of the signal after the laser pulse. Black dotted lines represent the fit obtained by using the MemExp program to calculate the continuous distributions $f(\tau)$ of lifetimes (for details, see text).

(b) Highly distributed kinetics are generally observed at low temperature in aqueous cryosolvent glasses [77] or at RT when the protein is embedded into trehalose glasses [14], due to the strongly retarded interconversion between conformational substates. Under these conditions, the trapping of the protein over a large ensemble of conformational energy minima, characterized by different reaction rates, can be observed on the timescale of the reaction.

In principle, the kinetics *N(t)* of Fig. 7 could be fitted to the sum of discrete exponential decays or power laws reflecting the contributions of charge recombination from any iron-sulfur cluster (F_X, F_A or F_B), as well as from the phylloquinone acceptors A_1 in each of the two symmetrical cofactor branches A and B [29, 40, 41]. However, we do not have any preliminary independent information on the number of kinetic phases, nor on the extent of their distribution. Unfortunately, several fitting solutions exist with different kinetic parameters, making such a fitting physically meaningless.

Therefore, we prefer to describe *N(t)* with a continuum distribution $f(\tau)$ of lifetimes τ, defined on a logarithmic scale [78],

$$N(t) = \int_{-\infty}^{\infty} d \log \tau \, f(\tau) \, e^{-t/\tau} \qquad (1)$$

and to obtain $f(\tau)$ by numerical inversion of Eq. 1. This strategy has the advantage that no *a priori* assumption is needed on the number of kinetic phases and on the functional form of the distribution. However, the numerical computation of $f(\tau)$, i.e., the inverse Laplace transformation of a set of kinetic data $N(t)$, that is inevitably noisy and incomplete, is ill-conditioned and can lead to significant ambiguity in $f(\tau)$ [79]. To overcome this problem, we inverted Eq. 1 by using in parallel two software packages (MemExp [67, 68, 80] and CONTIN [66]) based on different regularization algorithms (see Materials and Methods). By and large, the results of the MemExp and CONTIN kinetic analyses were rather similar, with some notable differences outlined further down in the text.

Figure 8 shows the lifetime distributions $f(\tau)$ corresponding to the kinetics $N(t)$ presented in Fig. 7, as obtained by using MemExp (panel A) and CONTIN (panel B). In an attempt to attribute individual peaks to specific recombination processes, each distribution has been fitted to the sum of Gaussian sub-distributions on a *log* τ scale. Examples of Gaussian decomposition of $f(\tau)$ for r = 11%, r = 43%, r = 63%, and in solution, as calculated by MemExp and by CONTIN, are given in Figs. S1 and S2 of Supplementary material. The parameters of the Gaussian components of $f(\tau)$ are summarized in Tables 1 and 2 for the distributions yielded by MemExp and CONTIN, respectively.

In solution, the lifetime distribution is dominated by a kinetic phase centered at τ ~100 ms, accounting for ~60-70% of the decay, which can be attributed to recombination from the $P_{700}^{\bullet+}[F_A/F_B]^{\bullet-}$ state [37]. The slowest Gaussian phase at τ ~0.5-0.6 s (phase 6 in Tables 1 and 2), can be ascribed to the reduction of $P_{700}^{\bullet+}$ by reduced DCPIP [37]. The presence of this very slow phase (see Fig. 7) is not surprising, since the procedure used to decrease the oxygen concentration in the liquid PS I suspension (see Materials and Methods) does not yield a fully anaerobic sample. Residual oxygen can subtract electrons from $[F_A/F_B]^{\bullet-}$ depriving of the recombination partner a fraction of $P_{700}^{\bullet+}$ that gets reduced by the exogenous DCPIP. In the distribution extracted by MemExp, two additional minor phases are present, peaking at τ ~3 ms and τ ~100 μs which, on the basis of their lifetimes, are ascribed to recombination from the $P_{700}^{\bullet+}F_X^{\bullet-}$ and $P_{700}^{\bullet+}A_1^{\bullet-}$ states, respectively [37].

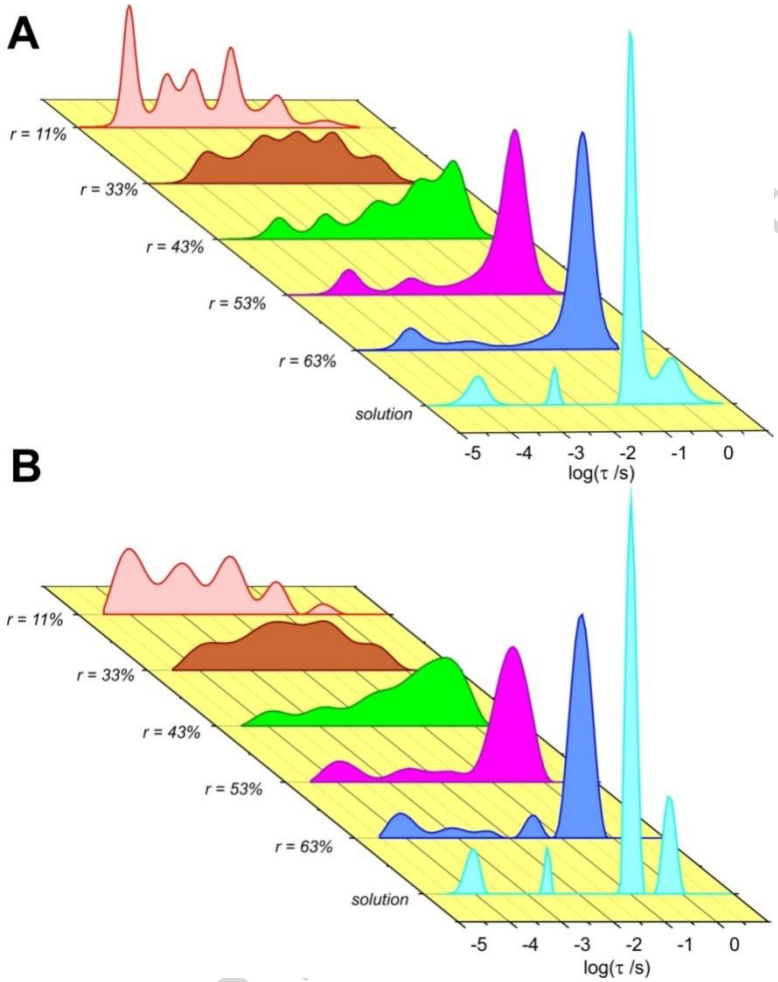

Figure 8. Evolution of the distribution functions $f(\tau)$ upon varying the hydration level (from $r = 11\%$ to $r = 63\%$) of the trehalose-PS I glass, as obtained by analyzing the decay kinetics in Fig. 7 by means of the MemExp (panel A) and CONTIN (panel B) programs. The distribution $f(\tau)$ calculated from the kinetics recorded in the PS I solution is shown for comparison. Normalization of the functions $f(\tau)$ is such that the integral of the probability over all possible values of τ is unity.

The kinetic component with $\tau \sim 100$ μs can be more specifically attributed to $P_{700}^{\bullet+}A_{1A}^{\bullet-}$, because the limited time resolution of our spectrometer (see Section 2.4) prevents the detection of possible contributions due to the recombination from $P_{700}^{\bullet+}A_{1B}^{\bullet-}$ along the B branch, which is characterized by $\tau \sim 10$ μs [25, 26, 33, 36, 81]. In the following, recombination from $P_{700}^{\bullet+}A_{1}^{\bullet-}$ will always refer to back-reaction along the A branch. The relative contributions of the two minor kinetic phases mentioned above (4% and 9%) are compatible with minor populations of the protein complex lacking the F_A/F_B and the F_X cofactors, respectively, as byproducts of the PS I isolation procedure. This is confirmed by similar phases revealed by CONTIN.

Table 1. Kinetic parameters obtained by fitting the distribution functions *f(τ)*, as calculated by the MemExp program (Fig. 8A), to the sum of Gaussian components.

r		Kinetic phase					
		1	2	3	4	5	6
11%	τ, ms	0.095	1.62 (0.498)[a]	8.38	54.8	557	
	fractional area	0.27	0.16 (0.17)[a]	0.23	0.14	0.03	
	σ, log(τ /ms)	0.128	0.171 (0.198)[a]	0.172	0.262	0.242	
33%	τ, ms	0.143	1.79	8.09	34.0	228	
	fractional area	0.14	0.37	0.11	0.25	0.14	
	σ, log(τ /ms)	0.261	0.453	0.200	0.290	0.294	
43%	τ, ms	0.154	1.19	12.2	80.4	364	
	fractional area	0.08	0.10	0.23	0.26	0.33	
	σ, log(τ /ms)	0.214	0.236	0.345	0.270	0.255	
53%	τ, ms	0.157	2.70		46.0	252	
	fractional area	0.09	0.08		0.13	0.70	
	σ, log(τ /ms)	0.221	0.328		0.347	0.246	
63%	τ, ms	0.111	1.19		53.7	250	
	fractional area	0.08	0.08		0.08	0.76	
	σ, log(τ /ms)	0.216	0.592		0.298	0.203	
solution	τ, ms	0.102	3.27			103	516
	fractional area	0.09	0.04			0.60	0.27
	σ, log(τ /ms)	0.190	0.069			0.093	0.364

[a] Values reported in brackets refer to the parameters of an additional Gaussian component, which has been tentatively associated with phase 2, attributed to $P_{700}^{\bullet+}F_X^{\bullet-}$ recombination.

The distribution *f(τ)* obtained in the most hydrated trehalose-PS I glassy matrix (*r* = 63%) is still dominated by a peak in the timescale of hundreds of ms (*τ* ~250 ms), attributed to $P_{700}^{\bullet+}[F_A/F_B]^{\bullet-}$ recombination. Similarly to what is observed for PS I solution, the *f(τ)* distribution obtained by MemExp exhibits also two faster minor phases, with τ in the timescale of 10^2 μs and 1 ms (see Table 1), ascribed to recombination from the $P_{700}^{\bullet+}A_1^{\bullet-}$ and $P_{700}^{\bullet+}F_X^{\bullet-}$ states, respectively. The CONTIN analysis yields comparable results. The contribution of the additional peak at *τ* ~4 ms is negligible (~1%) (see Table 2 and Fig. 8)). Both methods of analysis reveal a fourth Gaussian phase of small amplitude, at τ ~30-50 ms, which is ascribed to $P_{700}^{\bullet+}[F_A/F_B]^{\bullet-}$ recombination.

Table 2. Kinetic parameters obtained by fitting the distribution functions *f(τ)*, as calculated by the CONTIN program (Fig. 8B), to the sum of Gaussian components.

r		Kinetic phase					
		1	2	3	4	5	6
11%	τ, ms	0.095	0.957	9.00	66.0	556	
	fractional area	0.30	0.32	0.25	0.11	0.03	
	σ, log(τ /ms)	0.260	0.374	0.252	0.195	0.165	
33%	τ, ms	0.141	2.43	15.8	39.4	247	
	fractional area	0.14	0.45	0.11	0.18	0.12	
	σ, log(τ /ms)	0.344	0.564	0.414	0.336	0.295	
43%	τ, ms	0.121	1.06	16.6	78.0	318	
	fractional area	0.08	0.10	0.29	0.13	0.41	
	σ, log(τ /ms)	0.296	0.344	0.481	0.259	0.349	
53%	τ, ms	0.119	2.78	16.3	79.1	253	
	fractional area	0.11	0.09	0.03	0.05	0.72	
	σ, log(τ /ms)	0.308	0.375	0.217	0.204	0.301	
63%	τ, ms	0.076	0.787	3.66	28.1	243	
	fractional area	0.09	0.07	0.01	0.06	0.78	
	σ, log(τ /ms)	0.224	0.453	0.129	0.136	0.197	
solution	τ, ms	0.091	2.51			104	574
	fractional area	0.10	0.05			0.67	0.20
	σ, log(τ /ms)	0.129	0.053			0.094	0.114

It is noteworthy that several features of *f(τ)* differ significantly in the wet-glass and liquid samples: (a) The slowest peak detected in the solution, with τ ~0.5 s, disappears in the glass, indicating that reduction of $P_{700}^{\bullet+}$ by exogenous DCPIP does no longer occur. This probably reflects a decreased accessibility and/or reactivity of oxygen with the iron-sulfur centers in the trehalose glass. (b) The Gaussian phases ascribed to $P_{700}^{\bullet+}[F_A/F_B]^{\bullet-}$ and to $P_{700}^{\bullet+}F_X^{\bullet-}$ recombination become much broader in the glass (see Fig. 8 and Tables 1 and 2). This is consistent with the notion that thermal fluctuations between PS I conformational substates are strongly retarded in the trehalose glass. As a consequence, the averaging of the structural heterogeneity of the protein, taking place in solution on the timescale of electron-transfer, occurs to a much lesser extent in the glass, resulting in broader lifetime distributions. Such a broadening has been observed previously for the $P_{865}^{\bullet+}Q_A^{\bullet-}$ recombination kinetics in bacterial RCs embedded into dehydrated trehalose glasses [20]. (c) As compared to solution, the recombination kinetics of the $P_{700}^{\bullet+}[F_A/F_B]^{\bullet-}$ state is not only more distributed but also markedly slowed down in rate (see Fig. 8 and Tables 1 and 2). This suggests that the wet-trehalose glassy matrix primarily restricts the mobility of the outermost regions of the protein complex and increases the energy barriers governing the RT recombination rate ([25] and refs. therein). Note that a similar retardation of the $P_{700}^{\bullet+}$

$[F_A/F_B]^{\bullet-}$ recombination rate was observed at 230 K in the fully hydrated PS I complex (i.e., in a water-glycerol glass) [42].

When proceeding from hydrated (r = 63%) to extensively dehydrated conditions (r = 11%), the distribution undergoes deeper changes. Qualitatively the contribution of the faster phases increases at the expense of the slower ones (see Fig. 8). Under strongly dehydrated conditions (r <43%), the fastest peak (80 μs< τ<160 μs) becomes more pronounced.

In Tables 1 and 2, the parameters of the Gaussian components of $f(\tau)$ at the different hydration values have been aligned in five columns according to the respective peak lifetimes τ. As mentioned, phase 6 is only present in solution, and does not reflect any charge recombination. Based on previous analyses of charge recombination in solution [29, 40, 41], we suggest that phase 1 (τ ~100 μs) reflects $P_{700}^{\bullet+}A_1^{\bullet-}$ recombination, phases 2 and 3 (~0.5 to ~16 ms) represent recombination from $F_X^{\bullet-}$, and phases 4 and 5 recombination from $[F_A/F_B]^{\bullet-}$. Figure 9 shows the relative contributions of these phases, grouped as described above, as function of dehydration. Notably, the results based on CONTIN (squares) and MemExp (circles) analyses are largely similar. The contribution of the slowest phases (4 and 5) falls sharply at r <53%, simultaneously with the rise of the intermediate phases (2 and 3). The fastest phase 1 increases at r <43%.

The overall evolution of the lifetime distribution in the glass (Figs. 8 and 9) strongly suggests that dehydration of the matrix causes primarily a progressive arrest of forward electron transfer to F_A/F_B in an increasing fraction of the PS I population, as shown by the decrease in the contribution to the back reaction of the slowest phases (4 and 5). The increasing contribution, at r <43% , of the fastest phase suggests that, at lower content of residual water, also the forward electron transfer to F_X is blocked in an increasing PS I sub-population.

The kinetic phases attributed to the recombination from the $P_{700}^{\bullet+}F_X^{\bullet-}$ state (phases 2 and 3 with mean lifetimes of ~2 and ~10 ms, respectively) demonstrate a complex response to dehydration. The slower phase 3 contributes significantly to the kinetics only under dry conditions, at r ≤43%: At higher humidity, according to MemExp this phase is absent, and according to CONTIN its contribution is consistently negligible (<3%) (see Tables 1 and 2). At the lowest humidity, r = 11%, an additional phase, characterized by τ ~0.5 ms, is resolved by MemExp. This observation indicates a growing heterogeneity of the PS I conformational energy landscape. The heterogeneity may be caused by depletion or immobilization (see below) of water molecules belonging to one or both of the symmetrical intraprotein water clusters located between A_{1A}/A_{1B} and F_X [30], resulting in asymmetrical water allocation or dielectric properties in this protein region. Since at RT recombination from $P_{700}^{\bullet+}F_X^{\bullet-}$ most likely occurs through thermal repopulation of A_{1A}/A_{1B} [38] rather than directly to

$P_{700}^{\bullet+}$ heterogeneous water clusters between F_X and A_1 may promote preferable recombination through either A_{1A} or A_{1B}, resulting in several PS I subpopulations with distinct observable kinetic components.

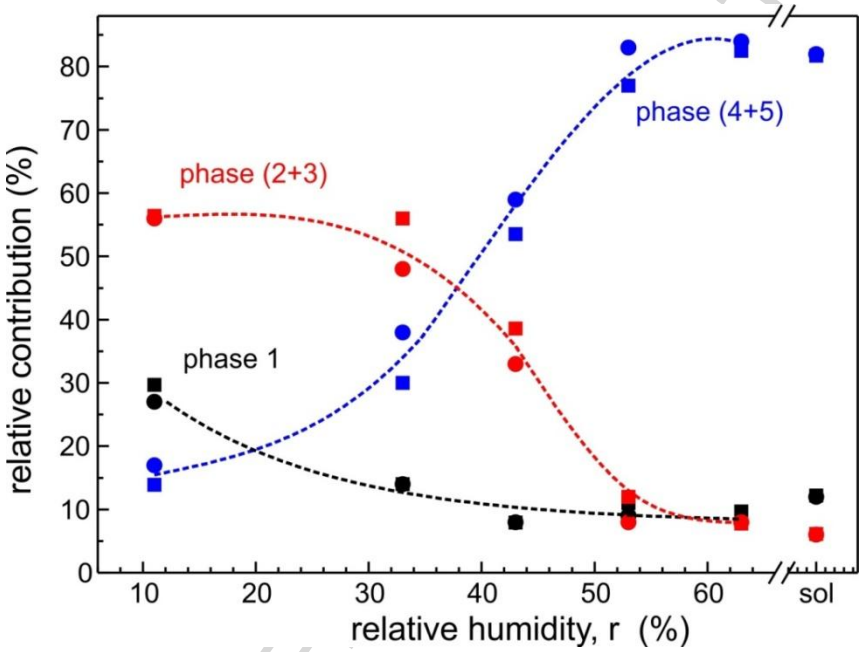

Figure 9. Relative contribution to charge recombination of the different phases of the distribution functions $f(\tau)$ given in Fig. 8, as a function of the relative humidity r. At each r value, $f(\tau)$ has been fitted to the sum of Gaussian sub-distributions (see Tables 1 and 2 for the values of the best fitting parameters). The label *sol* stands for solution. The relative contributions of the fastest phase (phase 1 in Tables 1 and 2) are represented by black symbols. Red symbols correspond to the sum of the normalized areas of phases 2 and 3; blue symbols represent the sum of the relative contribution of phases 4 and 5. Circles and squares refer to the results obtained by the MemExp and CONTIN programs, respectively. Dashed lines are drawn through the experimental points to guide the eye.

As to the recombination from the $P_{700}^{\bullet+}[F_A/F_B]^{\bullet-}$ state, two distinct phases are present at all levels of hydration (phases 4 and 5 in Tables 1 and 2, with mean lifetimes of ~56 ms and ~330 ms). As discussed above, at r <53%, the total contribution of these phases decreases (Fig. 9). Interestingly, following dehydration from r = 63% to 33%, the amplitude of phase 4 increases at the expense of phase 5 (see Tables 1 and 2). The electron balance between F_A and F_B clusters is not clearly understood yet, which makes it difficult to ascribe recombination kinetic phases to the back reaction from one or the other cluster [40]. However, it seems reasonable to associate the appearance of the faster phase 4 in the trehalose glass with recombination from the proximal cluster F_A. The increase in the contribution of this phase at the expense of the slower phase 5, which can be attributed to the distal

cluster F_B, suggests that progressive dehydration of the matrix precludes primarily the reduction of the distal F_B center, and only under the driest conditions the electron transfer to the proximal F_A cluster is blocked. This is consistent with the expectation (see below) that hardening of the hosting trehalose matrix upon dehydration reduces primarily the dynamics of outer protein regions closer to the protein-matrix interface.

In general, the effects of trehalose-matrix dehydration on the charge recombination resemble those observed in a glycerol-water mixture upon decreasing the temperature down to cryogenic values. At 77 K, about 45% of the photoinduced $P_{700}^{\bullet+}$ signal decayed in the submillisecond time domain; this kinetic component was attributed to a PS I subpopulation frozen in a conformational substate for which electron transfer to F_X is blocked [40]. A second PS I fraction (20%) was identified at 77 K, in which charge recombination occurred with complex kinetics from the $P_{700}^{\bullet+}F_X^{\bullet-}$ state [40]. In the remaining PS I population (~35%), formation of $P_{700}^{\bullet+}[F_A/F_B]^{\bullet-}$ was reported [40], irreversible on the time-scale of hours. Irreversible light-induced generation of the $P_{700}^{\bullet+}[F_A/F_B]^{\bullet-}$ state along the B branch of cofactors has been recently confirmed at cryogenic temperatures, involving ~35 - 50% of the PS I population [36]. Similar to what was observed in water-glycerol at cryogenic temperatures, in our RT study, under the driest condition (r = 11%) of the trehalose matrix, the forward electron transfer from the photoreduced phylloquinones $A_1^{\bullet-}$ to the iron-sulfur centers is prevented in ~30% of the PS I population. In 55%, recombination occurs from the $P_{700}^{\bullet+}F_X^{\bullet-}$ state with a strongly distributed heterogeneous kinetics, while in the remaining fraction (15%) $P_{700}^{\bullet+}[F_A/F_B]^{\bullet-}$ recombination takes place. At variance with low-temperature studies, we did not detect any significant changes in the total amplitude of the flash-induced absorption changes upon dehydration and rehydration of the samples (not shown), which reveals a lack of irreversible electron transfer to F_AF_B.

The appearance of subpopulations, characterized by distinct distributed electron transfer kinetics or even by inhibition of specific electron transfer steps (inhomogeneous inhibition), appears to be a general phenomenon, observable in photosystems embedded in dehydrated trehalose matrices at room temperature as well as in low-temperature glycerol-water glasses. The current interpretation for this behavior rests on the notion that proteins have a large number of conformational substates, many of which are almost iso-energetic (static structural heterogeneity) (for a review, see e.g. [82]). In RT solutions the protein rapidly samples this complex energy landscape by continuous jumps among the different conformations, thus averaging its static structural and kinetic heterogeneities. In low-temperature hydrated glasses or in RT dehydrated trehalose matrices, due to inhibition of interconversion between conformational substates, thermal averaging is hampered, giving rise to

distributed kinetics and freezing the protein over different conformational states, which will result in kinetically distinct subpopulations.

The close similarity between the effects of low temperatures on electron transfer in PS I water-glycerol systems and the effects of dehydration in RT trehalose-PS I glasses has been previously observed in the case of bacterial RCs [19]. The analogous effects observed in dehydrated trehalose-RC and trehalose-PS I glasses show that in both photosystems the protein conformational dynamics play a critical role in promoting forward electron transfer to the final acceptors. It has been in fact firmly established that dehydration of the trehalose-protein glass leads to a progressive reduction of protein conformational dynamics, caused by the dynamical coupling between the protein and the increasingly stiffened sugar matrix [19-21, 52, 76] (see Introduction). In particular, it has been proposed [9, 24] that the protein-matrix coupling is governed by a network of hydrogen bonds that connect surface protein residues and matrix trehalose molecules, mainly involving residual water molecules as mediators at the protein-matrix interface. Such a network of multiple H-bonds tightly locks the protein surface to the solid matrix under extensive dehydration (*anchorage hypothesis*) [9, 10, 24]. The surface constraints propagate into the interior of the protein through residue-residue and protein-cofactor interactions, also involving bound water molecules located in protein clefts and channels. The internal protein rigidity is therefore expected to be shaped by the hydration of the trehalose glass in such a way that the dynamics of the peripheral protein regions, close to the trehalose-coated protein surface, are more strongly hindered even in relatively wet glassy matrices, and that only a higher stiffening of the protein surface, at very low contents of residual water, may eventually affect the dynamics of the inner regions of the complex.

The effects of dehydration observed in the trehalose-PS I system appear consistent with this view. In fact, even a moderate dehydration (63%< r <43%) affects the electron-transfer processes which involve the terminal Fe_4S_4 clusters F_A and F_B, bound to the peripheral protein subunit PsaC: Incorporation of PS I into the trehalose glass at r = 63% significantly slows down recombination from the $P_{700}^{\bullet+}[F_A/F_B]^{\bullet-}$ state. And, at lower hydration (r = 43%), forward electron transfer from the photoreduced F_X center, located on the interface between PsaC and the heterodimer of PsaA and PsaB, appears to be blocked in ~40% of the PS I population (see Fig. 9).

As expected, only under more extensive dehydration of the matrix the electron-transfer reactions involving the redox cofactors located more deeply inside the protein are affected: (i) The electron transfer from the photoreduced phylloquinone $A_1^{\bullet-}$ to F_X is inhibited; (ii) The heterogeneity of recombination from the $P_{700}^{\bullet+}F_X^{\bullet-}$ state becomes more pronounced. These effects may be related to the smaller amount of water molecules and the larger hydrophobicity of the inner protein domains in PS I [83]. It is worth mentioning that effects (i) and (ii) appear at r <43%, when a change in the slope of the

water absorption isotherm is observed (see section 3.1 and Fig. S3). Below r = 43% the removal of residual water appears to be hindered, showing that water molecules more tightly bound to the trehalose matrix and/or to the protein are being removed.

The lifetime of $P_{700}^{\bullet+}A_1^{\bullet-}$ recombination increases upon decreasing the temperature, from <0.15 ms at RT [37] to ~0.3 ms at 77 K [40, 84]. In contrast, no systematic changes are detected upon dehydration of the trehalose-PS I matrix, both with regard to lifetime and distribution width of this electron-transfer process (see Fig. 8 and Tables 1 and 2). This is consistent with the observation that the W-band EPR spectrum of the spin-correlated $P_{700}^{\bullet+}A_1^{\bullet-}$ radical pair is insensitive to incorporation of PS I into the dehydrated trehalose matrix, indicating that the molecular configuration of the transient radical pair is not altered. We take the view that also the dynamics of the innermost region of the large PS I complex, where the binding site of the quinone cofactor is located, is not significantly affected by the trehalose matrix, even at the lowest hydration level tested in our study. Alternatively, this observation could reflect a very limited involvement of internal protein dynamics in $P_{700}^{\bullet+}A_1^{\bullet-}$ charge recombination, consistent with the high rigidity of the protein environment hosting these cofactors, as probed by molecular dynamics simulations [35].

To explain the heterogeneity of PS I electron transfer at cryogenic temperature and, in particular, the inhibition of forward electron transfer to the iron-sulfur centers, models have been proposed, which involve a distribution of conformational substates. They differ in the free energy of the radical pairs, as well as in the freezing of nuclear coordinates coupled to the electron-transfer process, resulting in modifications of the associated free energy change [25, 81]. In line with such a proposal, the appearance of heterogeneous electron transfer was found to correlate with the glass-transition temperature of the medium [40]. The results of our study, performed in room-temperature glasses, unambiguously demonstrate the critical role of conformational dynamics in governing electron transfer to the iron-sulfur centers.

The hindering of PS I dynamics by dehydration of the trehalose-PS I matrix can cause an inhomogeneous inhibition of forward electron transfer through specific, not mutually exclusive, mechanisms: (i) The freezing of nuclear coordinates associated with non-adiabatic medium reorganization results in an unfavorable free-energy change for electron transfer [25]; (ii) The block of adiabatic protein relaxations energetically destabilizes the photoreduced iron-sulfur acceptors; (iii) The increase of activation barriers, possibly induced by mechanisms (i) and (ii), prevents forward electron transfer beyond A_1 [39]; (iv) The dielectric properties of the protein are altered due the structural and dynamical modifications of the protein hydration shell and related changes of the hydrogen-bond network in the immediate environment of the iron-sulfur clusters. This could affect the redox potential of the cofactor, resulting in free-energy changes of forward electron transfer; (v) The heterogeneous

immobilization (or even partial deletion) of water molecules from the clusters around A_1 and F_X may play a role in the dielectric stabilization of the photoreduced F_X. Since the dynamics of the protein and its hydration shell are thought to be intimately connected (see e.g., [85]), the relaxational dynamics considered above (points (i) - (v)) are strictly correlated and are likely to be concomitantly affected in the trehalose glass matrix.

Recent theoretical work on the dynamics of intraprotein electron transfer has focused on the electrostatics of the protein-water interface [86, 87]. Molecular dynamics simulations have shown that hydrated redox-active proteins are specifically characterized by large-scale dipolar fluctuations of the hydration water, which correlate with fluctuations of the protein dipole. Additionally electrostatic fluctuations, dominated by a slow (~1 ns) component, are highly non-Gaussian and freeze at the temperature of the dynamical transition of proteins [87]. These properties of the protein-water interface have been proposed to largely control the energetics of electron transfer processes occurring on the ns timescale and above [86]. Interestingly, this is the timescale of forward electron transfer to the iron-sulfur centers, which we found to be inhomogeneosly blocked when the dynamics of the hydration shell is progressively frozen within the dehydrated trehalose glass.

4 Conclusions

A first systematic spectroscopic study of the large trimeric PS I membrane protein complex embedded in trehalose matrix under controlled hydration conditions has been presented. The reported NIR and high-field EPR results demonstrate that the dehydrated trehalose matrix of PS I strongly affects those slow collective protein internal motions that are coupled to long-range electron transfer. This suggests that the strong dynamical constraints, introduced at the surface of the protein-detergent complex by interactions with the trehalose sugar matrix, propagate over long distances (several nm) to the inner regions of a large protein complex. The hydration state of the trehalose matrix governs both its rigidity and the protein-matrix dynamical coupling, so that two hydration regimes can be identified: (a) At residual water contents between ~0.14 g and ~0.07 g of water per g of dry matrix, only electron transfer is affected involving the terminal iron-sulfur acceptors F_A/F_B, bound to the peripheral subunit PsaC. In strongly hydrated glasses (r = 63%), the only matrix effect is a slowing down of the recombination from the $P_{700}^{\bullet+}[F_A/F_B]^{\bullet-}$ state. Dehydration below ~0.11 g per g of dry matrix blocks the forward electron transfer from $F_X^{\bullet-}$ to F_A/F_B in an increasing fraction of the PS I population. (b) Below ~0.07 g of water per g of dry matrix, the electron transfer from $A_1^{\bullet-}$ to F_X also becomes hindered in a significant fraction of PS I, and a stronger heterogeneity appears in the kinetics of $P_{700}^{\bullet+}F_X^{\bullet-}$ recombination. At maximum dehydration tested (~0.025 g of water per g of dry matrix), in ~30% of

the PS I population charge separation is limited to the formation of the $P_{700}^{\bullet+}A_1^{\bullet-}$ state, similar to that observed in the hydrated PS I complex at cryogenic temperatures.

The overall response of PS I electron transfer to matrix dehydration resembles in many aspects that previously observed in the bacterial RC [19, 20]: A moderate progressive dehydration of RC-trehalose glasses also led to inhomogeneous inhibition of the forward electron transfer to the terminal quinone acceptor Q_B, and only extensive drying affected the stabilization of the primary charge-separated state $P_{865}^{\bullet+}Q_A^{\bullet-}$. In the case of PS I, however, the recombination lifetime of the $P_{700}^{\bullet+}A_1^{\bullet-}$ state was essentially unaffected by matrix dehydration, possibly due to the larger dimensions of the protein complex and/or to the high rigidity and low dielectric constant of the intervening inner protein region. This would minimize the effects of the trehalose matrix which is known to mainly affect large-amplitude, anharmonic conformational dynamics.

The results of this RT trehalose-PS I study strongly support the notion that protein/solvent dynamics play an essential role in electron transfer from the photoreduced A_1 cofactor to the iron-sulfur clusters. Our data suggest that photoreduction of the terminal acceptors is stabilized by dielectric relaxation and fast interconversion among PS I conformational substates. The different conformers, trapped at RT in extensively dehydrated trehalose glasses, are unlikely to reflect local heterogeneities of the glass matrix. This is because the W-band high-field EPR spectrum of a nitroxide spin probe, dispersed in dehydrated trehalose-PS I glasses, demonstrates a highly homogeneous structural organization of the protein-sugar matrix. The different conformers immobilized ("frozen") in dry RT trehalose glass appear, therefore, to reflect the genuine static heterogeneity of the PS I complex, which was previously suggested by low-temperature studies of the hydrated system in an aqueous cryosolvent [25]. As compared to low-temperature studies in the hydrated PS I complex, the use of dehydrated trehalose matrices has allowed us to trap at RT new conformers, in which most likely forward electron transfer to either F_A or F_B occurs, and recombination pathways from $P_{700}^{\bullet+}F_X^{\bullet-}$ along the A- or B-branch of the protein complex can be kinetically distinguished. Additionally, the W-band EPR spectra of the spin-correlated $P_{700}^{\bullet+}A_1^{\bullet-}$ radical pair convincingly show that incorporation into the trehalose matrix and its dehydration does not distort significantly the molecular configuration of the primary charge-separated state.

Remarkably, as shown by the full reversibility of the observed matrix effects, the PS I complex within the trehalose glass retains its structural and functional integrity for at least several months at room temperature. Thus, the trehalose matrix provides a convenient, stable system for studying function-dynamics relationships of large protein complexes under controlled water content of the microenvironment.

We emphasize that photosynthetic reaction centers, and in particular PS I, are optimal protein systems for an understanding of the role of different protein motional modes on protein function. They exhibit in fact a series of electron transfer processes, which can be followed easily, and which operate on different time scales, from sub-picoseconds to seconds. Low-frequency modes of proteins are particularly interesting, because they are related to functional properties. For example, it is believed that low-frequency collective modes are responsible for conformational energy and electron transfer in many biological processes. The coupling between such electron transfer processes and specific protein dynamics can be ideally investigated by incorporating the protein into room-temperature trehalose glasses. Dried trehalose matrices have been shown to affect selectively different protein motions: Large scale, anharmonic motions are more strongly reduced than faster harmonic vibrations, as revealed by Mössbauer spectroscopy [11] and neutron scattering studies performed in trehalose-coated co-ligated myoglobin [12].

In the light of these observations the results of the present study suggest that electron transfer to the terminal acceptors is primarily governed by collective low-frequency modes. We expect that information on the role of faster motional modes, in particular involving water molecules, will be provided by additional studies focused on fast primary electron transfer processes. Fast EPR and optical experiments along these lines, on bacterial RC and PS I complexes, are in progress in our laboratories.

The studies on function/dynamics relationship discussed in the present work and continued in our on-going work are embedded in the fundamental issue of what is the role water plays to sustain the biochemistry of the living cell. Over the past few decades it has become clear that water is not simply "life's solvent", but is indeed a matrix that actively interacts with biomolecules in complex ways for survival. The rationale for the distinguished role of molecular water in proteins rests on the spatially extended network of hydrogen bonds interacting with the surface of the protein. By modulating the interface between protein and solvent matrix, a new type of water is generated, "interface water" of the hydration shell, with properties fundamentally different from "bulk water", i.e., normal liquid water [88]. There is good physical reason to regard the solvent-solute interactions, and the way they shape and manipulate the hydration shell, as essential ingredients for protein function. We conclude by quoting Philip Ball at *Nature* [89]: "Moreover, the structure and dynamics of this hydration shell seem to feed back onto … the proteins themselves so that biological function depends on a delicate interplay between what we have previously regarded as distinct entities: the molecule and its environment. Many proteins make use of bound water molecules as functional units … to mediate interactions with other proteins or … to transport protons [and electrons] rapidly to locations buried inside the protein."

Acknowledgments

This work was financially supported by MIUR of Italy (to G. V.), by Russian Foundation for Basic Research, grant 15-04-04252 and Russian Science Foundation, grant 14-14-00789 (to A.Yu. S.), and by the Cluster of Excellence RESOLV (EXC 1069) funded by the Deutsche Forschungsgemeinschaft (to A. S.) and the Max Planck Society (to W. L. and K. M.). K. M. acknowledges sustaining support by the Free University Berlin. We want to thank Dmitry Cherepanov (Moscow State University) and John Golbeck (Pennsylvania State University) for stimulating and fruitful discussions.

References

[1] J.F. Carpenter, L.M. Crowe, J.H. Crowe, Stabilization of phosphofructokinase with sugars during freeze-drying. Characterization of enhanced protection in the presence of divalent cations, Biochim. Biophys. Acta, 923 (1987) 109-115.
[2] E.C. Lopez-Diez, S. Bone, The interaction of trypsin with trehalose: an investigation of protein preservation mechanisms, Biochim. Biophys. Acta, Gen. Subj., 1673 (2004) 139-148.
[3] N.K. Jain, I. Roy, Effect of trehalose on protein structure, Prot. Sci., 18 (2009) 24-36.
[4] S. Ohtake, Y.J. Wang, Trehalose: Current use and future applications, J. Pharm. Sci., 100 (2011) 2020-2053.
[5] J.H. Crowe, J.F. Carpenter, L.M. Crowe, The role of vitrification in anhydrobiosis, Annu. Rev. Physiol., 60 (1998) 73-103.
[6] L.M. Crowe, Lessons from Nature: The role of sugars in anhydrobiosis, Comp. Biochem. Physiol., Part A: Mol. Integr. Physiol., 131 (2002) 505-513.
[7] I.V. Shelaev, F.E. Gostev, M.D. Mamedov, O.M. Sarkisov, V.A. Nadtochenko, V.A. Shuvalov, A.Y. Semenov, Femtosecond primary charge separation in Synechocystis sp PCC 6803 photosystem I, Biochim. Biophys. Acta, Bioenerg., 1797 (2010) 1410-1420.
[8] L.Q. Chang, D. Shepherd, J. Sun, D. Ouellette, K.L. Grant, X.L. Tang, M.J. Pikal, Mechanism of protein stabilization by sugars during freeze-drying and storage: Native structure preservation, specific interaction, and/or immobilization in a glassy matrix?, J. Pharm. Sci., 94 (2005) 1427-1444.
[9] L. Cordone, G. Cottone, S. Giuffrida, G. Palazzo, G. Venturoli, C. Viappiani, Internal dynamics and protein-matrix coupling in trehalose-coated proteins, Biochim. Biophys. Acta, Proteins Proteomics, 1749 (2005) 252-281.
[10] L. Cordone, G. Cottone, A. Cupane, A. Emanuele, S. Giuffrida, M. Levantino, Proteins in saccharides matrices and the trehalose peculiarity: Biochemical and biophysical properties, Curr. Org. Chem., 19 (2015) 1684-1706.
[11] L. Cordone, P. Galajda, E. Vitrano, A. Gassmann, A. Ostermann, F. Parak, A reduction of protein specific motions in co-ligated myoglobin embedded in a trehalose glass, Eur. Biophys. J., 27 (1998) 173-176.
[12] L. Cordone, M. Ferrand, E. Vitrano, G. Zaccai, Harmonic behavior of trehalose-coated carbon-monoxy-myoglobin at high temperature, Biophys. J., 76 (1999) 1043-1047.
[13] G. Cottone, L. Cordone, G. Ciccotti, Molecular dynamics simulation of carboxy-myoglobin embedded in a trehalose-water matrix, Biophys. J., 80 (2001) 931-938.
[14] S.J. Hagen, J. Hofrichter, W.A. Eaton, Protein reaction kinetics in a room-temperature glass, Science, 269 (1995) 959-962.
[15] S.J. Hagen, J. Hofrichter, W.A. Eaton, Geminate rebinding and conformational dynamics of myoglobin embedded in a glass at room temperature, J. Phys. Chem., 100 (1996) 12008-12021.
[16] G. Feher, J.P. Allen, M.Y. Okamura, D.C. Rees, Structure and functioin of bacterial photosynthetic reaction centers, Nature, 339 (1989) 111-116.

[17] M.S. Graige, G. Feher, M.Y. Okamura, Conformational gating of the electron transfer reaction $Q_A^-Q_B \rightarrow Q_AQ_B^-$ in bacterial reaction centers of *Rhodobacter sphaeroides* determined by a driving force assay, Proc. Natl. Acad. Sci. U.S.A., 95 (1998) 11679-11684.
[18] J.D. McElroy, D.C. Mauzerall, G. Feher, Characterization of primary reactants in bacterial photosynthesis. II. Kinetic studies of the light-induced EPR signal (g = 2.0026) and the optical absorbance changes at cryogenic temperatures, Biochim. Biophys. Acta, 333 (1974) 261-278.
[19] F. Francia, G. Palazzo, A. Mallardi, L. Cordone, G. Venturoli, Residual water modulates Q_A^--to-Q_B electron transfer in bacterial reaction centers embedded in trehalose amorphous matrices, Biophys. J., 85 (2003) 2760-2775.
[20] G. Palazzo, A. Mallardi, A. Hochkoeppler, L. Cordone, G. Venturoli, Electron transfer kinetics in photosynthetic reaction centers embedded in trehalose glasses: Trapping of conformational substates at room temperature, Biophys. J., 82 (2002) 558-568.
[21] F. Francia, G. Palazzo, A. Mallardi, L. Cordone, G. Venturoli, Probing light-induced conformational transitions in bacterial photosynthetic reaction centers embedded in trehalose-water amorphous matrices, Biochim. Biophys. Acta, Bioenerg., 1658 (2004) 50-57.
[22] D. Kleinfeld, M.Y. Okamura, G. Feher, Electron-transfer kinetics in photosynthetic reaction centers cooled to cryogenic temperatures in the charge-separated state: evidence for light-induced structural changes, Biochemistry, 23 (1984) 5780-5786.
[23] B.H. McMahon, J.D. Muller, C.A. Wraight, G.U. Nienhaus, Electron transfer and protein dynamics in the photosynthetic reaction center, Biophys. J., 74 (1998) 2567-2587.
[24] F. Francia, M. Dezi, A. Mallardi, G. Palazzo, L. Cordone, G. Venturoli, Protein-matrix coupling/uncoupling in "dry" systems of photosynthetic reaction center embedded in trehalose/sucrose: The origin of trehalose peculiarity, J. Am. Chem. Soc., 130 (2008) 10240-10246.
[25] K. Brettel, Electron transfer and arrangement of the redox cofactors in photosystem I, Biochim. Biophys. Acta, Bioenerg., 1318 (1997) 322-373.
[26] K. Brettel, W. Leibl, Electron transfer in photosystem I, Biochim. Biophys. Acta, Bioenerg., 1507 (2001) 100-114.
[27] P. Fromme, P. Jordan, N. Krauss, Structure of photosystem I, Biochim. Biophys. Acta, Bioenerg., 1507 (2001) 5-31.
[28] P. Fromme, P. Mathis, Unraveling the Photosystem I reaction center: a history, or the sum of many efforts, Photosynth. Res., 80 (2004) 109-124.
[29] M. Mamedov, Govindjee, V. Nadtochenko, A. Semenov, Primary electron transfer processes in photosynthetic reaction centers from oxygenic organisms, Photosynth. Res., 125 (2015) 51-63.
[30] P. Jordan, P. Fromme, H.T. Witt, O. Klukas, W. Saenger, N. Krauss, Three-dimensional structure of cyanobacterial photosystem I at 2.5 angstrom resolution, Nature, 411 (2001) 909-917.
[31] M. Guergova-Kuras, B. Boudreaux, A. Joliot, P. Joliot, K. Redding, Evidence for two active branches for electron transfer in photosystem I, Proc. Natl. Acad. Sci. U.S.A., 98 (2001) 4437-4442.
[32] S. Santabarbara, P. Heathcote, M.C.W. Evans, Modelling of the electron transfer reactions in Photosystem I by electron tunnelling theory: The phylloquinones bound to the PsaA and the PsaB reaction centre subunits of PSI are almost isoenergetic to the iron-sulfur cluster Fx, Biochim. Biophys. Acta, Bioenerg., 1708 (2005) 283-310.
[33] N. Srinivasan, J.H. Golbeck, Protein-cofactor interactions in bioenergetic complexes: The role of the A_{1A} and A_{1B} phylloquinones in Photosystem I, Biochim. Biophys. Acta, Bioenerg., 1787 (2009) 1057-1088.
[34] J. Sun, S. Hao, M. Radle, W. Xu, I. Shelaev, V. Nadtochenko, V. Shuvalov, A. Semenov, H. Gordon, A. van der Est, J.H. Golbeck, Evidence that histidine forms a coordination bond to the A_{0A} and A_{0B} chlorophylls and a second H-bond to the A_{1A} and A_{1B} phylloquinones in $M688H_{PsaA}$ and $M668H_{PsaB}$ variants of *Synechocystis* sp. PCC 6803, Biochim. Biophys. Acta, Bioenerg., 1837 (2014) 1362-1375.
[35] G.E. Milanovsky, V.V. Ptushenko, J.H. Golbeck, A.Y. Semenov, D.A. Cherepanov, Molecular dynamics study of the primary charge separation reactions in Photosystem I: Effect of the replacement of the axial ligands to the electron acceptor A_0, Biochim. Biophys. Acta, Bioenerg., 1837 (2014) 1472-1483.
[36] H. Makita, G. Hastings, Directionality of electron transfer in cyanobacterial photosystem I at 298 and 77 K, FEBS Lett., 589 (2015) 1412-1417.
[37] I.R. Vassiliev, Y.S. Jung, M.D. Mamedov, A.Y. Semenov, J.H. Golbeck, Near-IR absorbance changes and electrogenic reactions in the microsecond-to-second time domain in photosystem I, Biophys. J., 72 (1997) 301-315.
[38] V.V. Ptushenko, D.A. Cherepanov, L.I. Krishtalik, A.Y. Semenov, Semi-continuum electrostatic calculations of redox potentials in photosystem I, Photosynth. Res., 97 (2008) 55-74.

[39] R. Agalarov, K. Brettel, Temperature dependence of biphasic forward electron transfer from the phylloquinone(s) A_1 in photosystem I: only the slower phase is activated, Biochim. Biophys. Acta, Bioenerg., 1604 (2003) 7-12.
[40] E. Schlodder, K. Falkenberg, M. Gergeleit, K. Brettel, Temperature dependence of forward and reverse electron transfer from A_1^-, the reduced secondary electron acceptor in photosystem I, Biochemistry, 37 (1998) 9466-9476.
[41] V. Shinkarev, Functional modeling of electron transfer in photosynthetic reaction centers, in: G. J. (Ed.) Photosystem I. The Light-Driven Plastocyanin:Ferredoxin Oxidoreductase, Springer, Dordrecht, 2006, pp. 611-637.
[42] R. Jordan, U. Nessau, E. Schlodder, Charge recombination between the reduced iron-sulphur clusters and P700, in: G. Garab (Ed.) Photosynthesis: Mechanisms and Effects, Vols I-V, 1998, pp. 663-666.
[43] R. Malkin, A.J. Bearden, Primary reactions of photosynthesis: photoreduction of a bound chloroplast ferredoxin at low temperature as detected by EPR spectroscopy, Proc. Natl. Acad. Sci. U.S.A., 68 (1971) 16-19.
[44] P. Setif, P. Mathis, T. Vanngard, Photosystem I photochemistry at low temperature. Heterogeneity in pathways for electron transfer to the secondary acceptors and for recombination processes, Biochim. Biophys. Acta, 767 (1984) 404-414.
[45] A.R. McIntosh, M. Chu, J.R. Bolton, Flash photolysis electron spin resonance studies of the electron acceptor species at low temperatures in photosystem I of spinach subchloroplast particles, Biochim. Biophys. Acta, 376 (1975) 308-314.
[46] R.I. Agalarov, Electron transfer in Photosystem I embedded in trehalose glass, Trans. Int. Acad. Sci., 3 (2009) 480-485.
[47] A. Semenov, M. Malferrari, A. Savitsky, M. Mamedov, K. Möbius, G. Venturoli, Effect of disaccharide trehalose glassy matrix on charge recombination in Photosystem I, in: K. Salikov (Ed.) Modern Development of Magnetic Resonance, Kazan, Russia, 2015, pp. 17.
[48] G.Z. Shen, J.D. Zhao, S.K. Reimer, M.L. Antonkine, Q. Cai, S.M. Weiland, J.H. Golbeck, D.A. Bryant, Assembly of photosystem II. Inactivation of the rubA gene encoding a membrane-associated rubredoxin in the cyanobacterium *Synechococcus* sp PCC 7002 causes a loss of photosystem I activity, J. Biol. Chem., 277 (2002) 20343-20354.
[49] D.I. Arnon, Copper enzymes in isolated chloroplasts. Polyphenoloxidase in *beta vulgaris*., Plant Physiol., 24 (1949) 1-15.
[50] A. Savitsky, A.A. Dubinskii, M. Plato, Y.A. Grishin, H. Zimmermann, K. Möbius, High-field EPR and ESEEM investigation of the nitrogen quadrupole interaction of nitroxide spin labels in disordered solids: Toward differentiation between polarity and proticity matrix effects on protein function, J. Phys. Chem. B, 112 (2008) 9079-9090.
[51] M. Malferrari, A. Nalepa, G. Venturoli, F. Francia, W. Lubitz, K. Möbius, A. Savitsky, Structural and dynamical characteristics of trehalose and sucrose matrices at different hydration levels as probed by FTIR and high-field EPR, Phys. Chem. Chem. Phys. , 16 (2014) 9831-9848.
[52] M. Malferrari, F. Francia, G. Venturoli, Retardation of protein dynamics by trehalose in dehydrated systems of photosynthetic reaction centers. Insights from electron transfer and thermal denaturation kinetics, J. Phys. Chem. B, 119 (2015) 13600-13618.
[53] M. Malferrari, F. Francia, G. Venturoli, Coupling between electron transfer and protein-solvent dynamics: FTIR and laser-flash spectroscopy studies in photosynthetic reaction center films at different hydration levels, J. Phys. Chem. B, 115 (2011) 14732-14750.
[54] L. Greenspan, Humidity fixed points of binary saturated aqueous solutions, J. Res. Natl. Bur. Stand. A., 814 (1977) 89-96.
[55] M. Giustini, G. Palazzo, G. Colafemmina, M. DellaMonica, M. Giomini, A. Ceglie, Microstructure and dynamics of the water-in-oil CTAB/n-pentanol/n-hexane/water microemulsion: A spectroscopic and conductivity study, J. Phys. Chem., 100 (1996) 3190-3198.
[56] W.F. McClure, H. Maeda, J. Dong, Y.L. Liu, Y. Ozaki, Two-dimensional correlation of Fourier transform near-infrared and Fourier Transform Raman spectra I: Mixtures of sugar and protein, Appl. Spectrosc., 50 (1996) 467-475.
[57] Y. Hattori, M. Otsuka, NIR spectroscopic study of the dissolution process in pharmaceutical tablets, Vib. Spectrosc., 57 (2011) 275-281.
[58] S.C. Straley, W.W. Parson, D.C. Mauzerall, R.K. Clayton, Pigment content and molar extinction coefficients of photochemical reaction centers from *Rhodopseudomonas spheroides*, Biochim. Biophys. Acta, 305 (1973) 597-609.

[59] A. Lerbret, F. Affouard, A. Hedoux, S. Krenzlin, J. Siepmann, M.C. Bellissent-Funel, M. Descamps, How strongly does trehalose interact with lysozyme in the solid state? Insights from molecular dynamics simulation and inelastic neutron scattering, J. Phys. Chem. B, 116 (2012) 11103-11116.
[60] B.J. Harris, X. Cheng, P. Frymier, All-atom molecular dynamics simulation of a Photosystem I/detergent complex, J. Phys. Chem. B, 118 (2014) 11633-11645.
[61] O. Burghaus, M. Rohrer, T. Götzinger, M. Plato, K. Möbius, A novel high-field high-frequency EPR and ENDOR spectrometer operating at 3 mm wavelength, Meas. Sci. Technol., 3 (1992) 765-774.
[62] T.F. Prisner, M. Rohrer, K. Möbius, Pulsed 95-GHz high-field EPR heterodyne spectrometer with high spectral and time resolution, Appl. Magn. Reson., 7 (1994) 167-183.
[63] K. Möbius, A. Savitsky, A. Schnegg, M. Plato, M. Fuchs, High-field EPR spectroscopy applied to biological systems: characterization of molecular switches for electron and ion transfer, Phys. Chem. Chem. Phys., 7 (2005) 19-42.
[64] S. Stoll, A. Schweiger, EasySpin, a comprehensive software package for spectral simulation and analysis in EPR, J. Magn. Reson., 178 (2006) 42-55.
[65] D.L. Phillips, A technique for the numerical solution of certain integral equations of the first kind, J. Assoc. Comput. Mach., 9 (1962) 84-97.
[66] S.W. Provencher, CONTIN: a general purpose constrained regularization program for inverting noisy linear algebraic and integral equations, Comput. Phys. Commun., 27 (1982) 229-242.
[67] P.J. Steinbach, R. Ionescu, C.R. Matthews, Analysis of kinetics using a hybrid maximum-entropy/nonlinear-least-squares method: Application to protein folding, Biophys. J., 82 (2002) 2244-2255.
[68] P.J. Steinbach, Filtering artifacts from lifetime distributions when maximizing entropy using a bootstrapped model, Anal. Biochem., 427 (2012) 102-105.
[69] P.R. Bevington, Data reduction and error analysis for the physical sciences, McGraw-Hill, New York, 1969.
[70] D. Stehlik, C.H. Bock, J. Petersen, Anisotropic electron-spin polarization of correlated spin pairs in photosynthetic reaction centers, J.Phys. Chem., 93 (1989) 1612-1619.
[71] P.J. Hore, Analysis of polarized EPR spectra, in: A.J. Hoff (Ed.) Advanced EPR. Applications in Biology and Biochemistry.
, Elsevier, 1989, pp. 405-440.
[72] A. Savitsky, M. Malferrari, F. Francia, G. Venturoli, K. Möbius, Bacterial photosynthetic reaction centers in trehalose glasses: Coupling between protein conformational dynamics and electron-transfer kinetics as studied by laser-flash and high-field EPR spectroscopies, J. Phys. Chem. B, 114 (2010) 12729-12743.
[73] F. Librizzi, C. Viappiani, S. Abbruzzetti, L. Cordone, Residual water modulates the dynamics of the protein and of the external matrix in "trehalose coated" MbCO: An infrared and flash-photolysis study, J. Chem. Phys., 116 (2002) 1193-1200.
[74] S. Giuffrida, G. Cottone, F. Librizzi, L. Cordone, Coupling between the thermal evolution of the heme pocket and the external matrix structure in trehalose coated carboxymyoglobin, J. Phys. Chem. B, 107 (2003) 13211-13217.
[75] S. Giuffrida, G. Cottone, L. Cordone, Structure-dynamics coupling between protein and external matrix in sucrose-coated and in trehalose-coated MbCO: An FTIR study, J. Phys. Chem. B, 108 (2004) 15415-15421.
[76] F. Francia, M. Malferrari, S. Sacquin-Mora, G. Venturoli, Charge recombination kinetics and protein dynamics in wild type and carotenoid-less bacterial reaction centers: Studies in trehalose glasses, J. Phys. Chem. B, 113 (2009) 10389-10398.
[77] A. Ansari, C.M. Jones, E.R. Henry, J. Hofrichter, W.A. Eaton, The role of solvent viscosity in the dynamics of protein conformational changes, Science, 256 (1992) 1796-1798.
[78] P.J. Steinbach, K. Chu, H. Frauenfelder, J.B. Johnson, D.C. Lamb, G.U. Nienhaus, T.B. Sauke, R.D. Young, Determination of rate distributions from kinetic experiments, Biophys. J., 61 (1992) 235-245.
[79] J.G. McWirther, E.R. Pike, On the numerical inversion of the Laplace transform and Fredholm integral equations of the first kind, J. Phys. A Math. Gen., 11 (1978) 1297-1745.
[80] P.J. Steinbach, Inferring lifetime distributions from kinetics by maximizing entropy using a bootstrapped model, J. Chem. Inf. Comp. Sci., 42 (2002) 1476-1478.
[81] S. Santabarbara, I. Kuprov, O. Poluektov, A. Casal, C.A. Russell, S. Purton, M.C.W. Evans, Directionality of electron-transfer reactions in Photosystem I of prokaryotes: Universality of the bidirectional electron-transfer model, J. Phys. Chem. B, 114 (2010) 15158-15171.
[82] H. Frauenfelder, B.H. McMahon, Energy landscape and fluctuations in proteins, Ann. Phys., 9 (2000) 655-667.

[83] S.K. Chamorovsky, D.A. Cherepanov, C.S. Chamorovsky, A.Y. Semenov, Correlation of electron transfer rate in photosynthetic reaction centers with intraprotein dielectric properties, Biochim. Biophys. Acta, Bioenerg., 1767 (2007) 441-448.
[84] H. Makita, N. Zhao, G. Hastings, Time-resolved visible and infrared difference spectroscopy for the study of photosystem I with different quinones incorporated into the A_1 binding site, Biochim. Biophys. Acta, Bioenerg., 1847 (2015) 343-354.
[85] H. Frauenfelder, G. Chen, J. Berendzen, P.W. Fenimore, H. Jansson, B.H. McMahon, I.R. Stroe, J. Swenson, R.D. Young, A unified model of protein dynamics, Proc. Natl. Acad. Sci. U.S.A., 106 (2009) 5129-5134.
[86] D.N. LeBard, D.V. Matyushov, Protein-water electrostatics and principles of bioenergetics, Phys. Chem. Chem. Phys., 12 (2010) 15335-15348.
[87] D.N. LeBard, D.V. Matyushov, Ferroelectric Hydration Shells around Proteins: Electrostatics of the Protein-Water Interface, J. Phys. Chem. B, 114 (2010) 9246-9258.
[88] S. Gekle, Wasser in Grenzen, Physik Journal, 11 (2015) 29-34.
[89] P. Ball, Water as an active constituent in cell biology, Chem. Rev., 108 (2008) 74-108.

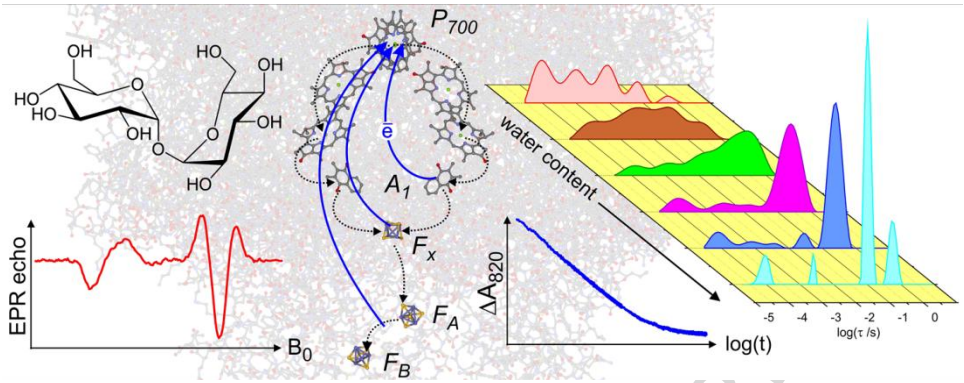

Graphical Abstract

Highlights

- Trimeric PS I can be functionally incorporated into trehalose glassy matrices.
- Charge recombination kinetics have been studied by W-band EPR and NIR spectroscopy.
- Dehydration inhibits at room temperature electron transfer to the [4Fe-4S] clusters.
- PS I conformational dynamics is required for efficient charge separation.
- PS I is stable at room temperature for months into dried trehalose matrices.